Reviews and syntheses: Recent advances in microwave remote sensing in support terrestrial carbon cycle science of arctic-boreal regions

Alex Mavrovic[1-2-3-4], Oliver Sonnentag[2-4], Juha Lemmetyinen[5], Jennifer L. Baltzer[6],
Christophe Kinnard[1-2], Alexandre Roy[1-2].

[1] Université du Québec à Trois-Rivières, Trois-Rivières, Québec, Canada
[2] Centre d'Études Nordiques, Université Laval, Québec, Québec, Canada
[3] Polar Knowledge Canada, Canadian High Arctic Research Station campus, Cambridge Bay, Nunavut, Canada
[4] Université de Montréal, Montréal, Québec, Canada
[5] Finnish Meteorological Institute, Helsinki, Finland
[6] Biology Department, Wilfrid Laurier University, Waterloo, Ontario, Canada

Correspondence to: Alex Mavrovic (alex.mavrovic@uqtr.ca)

Abstract. Spaceborne microwave remote sensing (300 MHz – 100 GHz) provides a valuable method for characterizing environmental changes, especially in arctic-boreal regions (ABR) where ground observations are generally spatially and temporally scarce. Although direct measurements of carbon fluxes are not feasible, spaceborne microwave radiometers and radar can monitor various important surface and near-surface variables that affect terrestrial carbon cycle processes such as respiratory carbon dioxide (CO_2) fluxes, photosynthetic CO_2 uptake, and processes related to net methane (CH_4) exchange including CH_4 production, transport, and consumption. Examples of such controls include soil moisture and temperature, surface freeze/thaw cycles, vegetation water storage, snowpack properties and land cover. Microwave remote sensing also provides a means for independent aboveground biomass estimates that can be used to estimate aboveground carbon stocks. The microwave data record spans multiple decades going back to the 1970s with frequent (daily to weekly) global coverage independent of atmospheric conditions and solar illumination. Collectively, these advantages hold substantial untapped potential to monitor and better understand carbon cycle processes across the ABR. Given rapid climate warming across the ABR and the associated carbon cycle feedbacks to the global climate system, this review argues for the importance of rapid integration of microwave information into ABR terrestrial carbon cycle science.

Keywords: Microwave remote sensing, Carbon cycle science, Carbon dioxide, Methane, Arctic-boreal regions

1 Introduction

Northern regions host two important terrestrial biomes, the boreal and the Arctic (hereafter called arctic-boreal regions; ABR). Belowground carbon (C) stocks in the ABR comprise 30-40% of the planetary

terrestrial carbon and as such, understanding changes in carbon cycle processes in this vast region has global importance (Pan et al., 2011; Tarnocai et al., 2009). Arctic-boreal regions store substantial quantities of belowground C due to their inherently slow decomposition rates, largely attributable to cold temperatures (Ravn et al., 2020). A large portion of the ABR is underlain by permafrost (perennially frozen ground), which contains approximately half of the world's belowground C stocks (1672 Pg C in the top three meters of soil; Tarnocai et al., 2009; van Huissteden and Dolman, 2012). In contrast, C stocks in above-ground biomass in the ABR are relatively trivial. For example, although the boreal biome constitutes the second-largest terrestrial biome with a third of the world's forested area, it contains only approximately 15 % of the global forest aboveground biomass (FAO, 2001; Pan et al., 2011 and 2013; Carreiras et al., 2017) but 32 % of the global forest carbon stocks (Pan et al., 2011).

Above- and belowground C pools in the ABR are vulnerable to climate change (Grosse et al., 2011). Arctic-boreal regions are warming at a disproportional rate compared to the rest of the planet with potential feedbacks to the global climate system (Box et al., 2019; Derksen et al., 2019; IPCC, 2019; Rantanen et al., 2022). In conjunction with warming temperatures, the ABR is experiencing altered precipitation regimes (Callaghan et al., 2011; Bokhorst et al. 2016; Dolant et al., 2018), permafrost thawing and deepening of the hydrologically and biogeochemically active layer (Liljedahl et al., 2016; Miner et al., 2022), spatially variable vegetation responses associated with 'greening' and 'browning' (i.e., increasing and decreasing productivity, respectively; Sulla-Menashe et al., 2018; Myers-Smith et al., 2020), earlier spring thaw, later freeze-up and lengthening of the growing season (Kimball et al., 2004a; Euskirchen et al., 2006; Kim et al., 2012), modifications of land cover (Wang at al., 2020), and intensifying disturbance regimes such as fire, drought, pervasive insect infestation and disease (Peng et al., 2011; Yi et al., 2013; Foster et al., 2022). Although ongoing warming has the potential to enhance photosynthesis and plant growth across the ABR, which would also increase above-ground C storage (Sturm et al., 2005; McMahon et al., 2010; Myers-Smith et al., 2020), the vegetation response to climate change is variable and complex. Furthermore, warmer air and soil temperatures enhance soil organic matter decomposition and subsequent release of carbon dioxide (CO_2) via respiration (Schädel et al., 2016). Large uncertainties remain in terrestrial biosphere models used to estimate CO_2 and CH_4 fluxes in the ABR (Tei and Sugimoto, 2020; Fisher et al., 2018, including the amount of CO_2 and CH_4 released during winter (Natali et al., 2019; Zona et al., 2015). If increases in ecosystem respiration exceed those of photosynthetic CO_2 uptake from enhanced plant growth, the ABR may shift from a weak net CO_2 sink to a net CO_2 source, thereby generating a potentially non-negligible, positive feedback to the global climate system. This potential change underlines the importance of understanding changes in ABR C pools and fluxes (Hayes et al. 2011; Schuur et al., 2015; Gauthier et al., 2015; Virkkala et al., 2021).

The vastness and remoteness of ABR make *in situ* observations challenging and costly. For example, although FLUXNET, the global initiative of tower-based eddy covariance flux observations (Baldocchi et al., 2001; Pastorello et al., 2020), is the most broadly used reference for C flux measurements at the ecosystem

scale, ABR are notoriously underrepresented in this network (Fig. 1; Baldocchi et al., 2001; Pastorello et al., 2020; Pallandt et al., 2022). Satellite remote sensing and terrestrial biosphere models show promise for monitoring land surface-atmosphere interactions across ABR (Fisher et al., 2018; Lees et al., 2018). Although direct measurement of C fluxes is not yet possible through remote sensing, it is possible to use spaceborne sensors to monitor variables and ecosystem structural parameters that exert control over various ecosystem processes (Du et al., 2019). In the last decade, radiometers sensitive to wavelengths in the visible and infrared portions of the electromagnetic spectrum have been used widely to support C cycle science in the ABR (Turner et al., 2004; Mao et al., 2016, Lees et al., 2018, Xiao et al. 2019). Visible and infrared remote sensing observations have been used in C cycle science to map spectral vegetation indices as proxies for vegetation abundance and productivity (e.g., normalized difference vegetation index [NDVI]; Tucker, 1979; Lees et al., 2018; Du et al., 2019), forest disturbance (e.g., fire, tree mortality; Kim et al., 2012), land cover (Kimball et al., 2009), vegetation structure (e.g., light detection and ranging [LiDAR]; Xiao et al., 2019), snow cover extent (Hori et al., 2017), land surface temperature (Sitch et al., 2007; Xiao et al., 2019), albedo (Xiao et al., 2019), solar-induced chlorophyll fluorescence (Wohlfahrt et al., 2018; Magney et al., 2019), and atmospheric CO_2 concentration (Buchwitz et al., 2007; Tu et al., 2020; Lorente et al., 2021). However, spaceborne visible and infrared radiometers are affected by signal degradation from atmospheric effects, have minimal signal penetration depth in vegetation, and depend on solar illumination meaning they are restricted to daytime, clear sky observations (Kim et al., 2012).
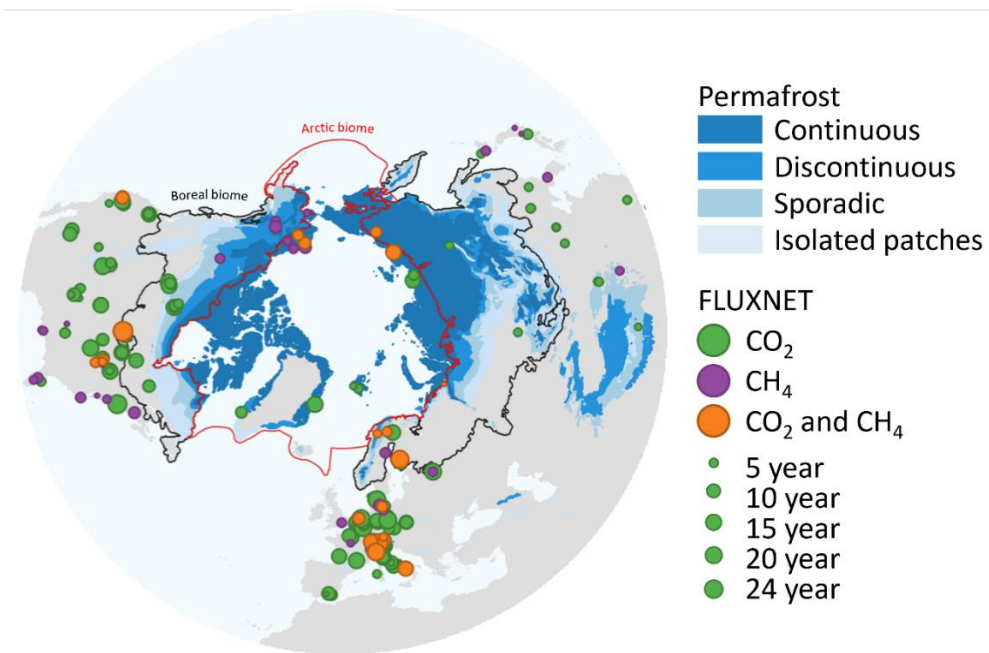
Figure 1: Permafrost extent (Brown et al., 2002) and distribution of eddy covariance sites where ecosystem fluxes are monitored continuously (Baldocchi et al., 2001 and Pallandt et al., 2022; dot size represents the number of years of available data). The Arctic biome is delineated following the Conservation of Arctic Flora and Fauna working group of the Arctic Council and the boreal biome is delineated following Potapov et al. (2008). Permafrost extent is estimated in percent areal coverage: continuous (>90-100 % areal extent), discontinuous (>50-90 %), sporadic (10-50 %) and isolated patches (<10 %).

Spaceborne microwave remote sensing can be used in synergy with visible and infrared radiometers to maximize the benefits of a wider frequency span in the electromagnetic spectrum (Sitch et al., 2007; Kimball et al., 2009; Arslan et al., 2011; Kim et al., 2012; Xiao et al., 2019). Microwaves encompass electromagnetic radiation within the frequency range of 0.3–300 GHz, which corresponds to wavelengths from 1 mm to 1 m. Microwave remote sensing provides several advantages such as its relative insensitivity to atmospheric attenuation, cloud cover, and solar illumination at frequencies below 100 GHz, which is essential during winter months in regions undergoing polar night (Sitch et al., 2007; Du et al., 2019). The spatial resolution of microwave imagery ranges from coarse (several-kilometer scale) to fine (meter scale) with varying temporal resolutions that can reach more than one observation per day. Microwave remote sensing is particularly suitable for the ABR since the signal penetration depth range allows the retrieval of (1) volumetric information such as certain snow properties including density and microstructure (e.g., Nagler and Rott, 2000; Takala et al., 2011; Lievens et al., 2019) and vegetation optical depth (VOD), which relates to aboveground biomass and vegetation liquid water content (Konings et al., 2017 and 2019; Mialon et al., 2020), as well as (2) near-surface information on variables such as soil moisture (Kerr et al., 2012; Colliander et al. 2017) and freeze/thaw state (Kim et al., 2012; Roy et al., 2015; Rautiainen et al., 2016; Derksen et al., 2017; Prince et al., 2019) because of its sensitivity to liquid water.

This paper aims to introduce to the C cycle science community the potential of spaceborne microwave remote sensing to help overcome some of the challenges specifically posed by the ABR for terrestrial C cycle science and monitoring. We focus on the main vertical C fluxes between the land surface and the atmosphere, specifically, respiratory CO_2 fluxes, photosynthetic CO_2 uptake, and processes related to net methane (CH_4) fluxes governed by CH_4 production, transport, and consumption. After summarizing the principles of microwave remote sensing (2), we review how spaceborne microwave remote sensing can be exploited to help monitor key variables important for CO_2 and CH_4 fluxes in the ABR. These include soil moisture (3.1) and temperature (3.2), surface freeze/thaw status (3.3), aboveground biomass (3.4), vegetation water status (3.5), landcover (3.6) and snow cover (3.7). For each variable, we will first explain how the variable at least partially governs C exchanges, outline the potential of microwave remote sensing to monitor the key variable, and then presently available microwave remote sensing products related to each variable.

2 Principles of microwave remote sensing

Microwave remote sensing can be used passively, by measuring the natural microwave emission from the planetary surface (using radiometers; receiving only), or actively, by measuring the backscattering of a previously emitted signal (using radar instruments; emitting and receiving).

Radiometers measure the natural microwave emission coming from the planetary surface. This emission is quantified as the brightness temperature (T_B; Fig. 2b), which corresponds to the temperature of a blackbody delivering the same luminance as the studied surface. Brightness temperature is related to the physical

135 temperature of a surface ($T_B = e \cdot T$) through emissivity (e; unitless). Emissivity is an inherent material property ranging from 0 for a perfectly non-emitting material, to 1 for a purely emitting material (blackbody). The microwave electric field generally displays a preferred orientation, called the microwave polarization, and is often related to the geometric structure of the source or target (Ulaby et al., 1982 and 1983). The spatial resolution of passive microwave radiometers is generally coarser than many visible and infrared radiometers

140 owing to the longer wavelengths and practical restrictions of the receiving antenna dimensions on spacecraft (Jenson, 2006). Spaceborne passive microwave radiometers typically have spatial resolutions in the 10- to 100-km range. Although passive microwave spatial resolutions are often too coarse to capture small-scale landscape heterogeneity (meter to kilometer scale), it is not an obstacle for regional or global applications of terrestrial biosphere models commonly run at spatial resolutions of several kilometers. The temporal

145 resolution of most microwave instruments is generally less than 2-3 days, and in polar regions several overpasses a day may be achieved. The fine temporal resolution might be more critical for terrestrial biosphere models than good spatial resolution since computational power limits the spatial resolution of such models (Washington et al., 2009; Schär et al., 2020).

150 Radars emit electromagnetic waves to calculate the backscattering coefficient (σ; Fig. 2b) of a target area from the power ratio between the emitted and returned pulse (Ulaby et al., 1982 and 1986). The return signal of a radar carries three main pieces of information, the magnitude of σ, the phase of the electromagnetic wave returning, and a delay between the emitted and received signal which is related to the distance between the radar and the target area. Scatterometers focus particularly on the magnitude of the backscattered signal

155 by a medium to extract backscattering coefficient (Figa-Saldaña et al., 2002). Synthetic aperture radar (SAR) measures backscattering coefficients using a radar technique that can achieve spatial resolutions at a meter scale by combining scenes of the target area from multiple points of view (Tomiyasu, 1978; Balmer, 2000). Synthetic aperture radars achieve comparable resolutions to visible and infrared radiometers (i.e., below 10 m of spatial resolution). However, radar transmitters are much more energy-consuming than radiometers

160 because of the power requirement for emitting microwaves. Because of high energy demands, most SAR transmitters operate during a small fraction (1-30 %; Gasso et al., 2021; Leanza et al., 2019; Dubock et al., 2001) of their orbit around the earth. The lower the transmission time, the greater the duration between measurements at a given point, often several days (Marghany, 2019). This is currently being overcome via deployment of several satellites equipped with SAR instruments flying in tandem (Sentinel-1; Radarsat

165 Constellation Mission).

Unlike visible and infrared remote sensing that are limited to information from the surface of any target, the longer wavelengths of microwave allow microwaves to penetrate vegetation, ground, and snowpack allowing subsurface measurements (Ulaby et al., 1986); the longer the microwave, the deeper the penetration

170 depth. However, deeper penetration means that the received signal is a combination of different contributing components, i.e., usually vegetation, soil, snow, and atmosphere (Kerr et al., 2012, Roy et al., 2012 and

2014), challenging the interpretation of the signal. Consequently, microwave remote sensing is often used together with radiative transfer models to decouple and extract the information on terrestrial surface conditions from microwave observations. These models generally calculate the scattering, reflection, and attenuation of the electromagnetic waves of the different components of the surface (Fig. 2) (Mo et al., 1982; El-Rayes and Ulaby, 1987; Huang et al., 2017; Picard et al., 2018). By considering the contribution of each component of the surface (i.e., soil, vegetation and/or snow), radiative transfer models allow disentangling microwave signals to retrieve key surface state variables of interest (Wigneron et al., 2007).

(a) Passive microwave

$$T_B = e\gamma T_{soil} + (1-\omega)(1-\gamma)T_{veg} + (1-\omega)(1-\gamma)(1-e)\gamma T_{veg}$$
$$\quad\quad (1)\quad\quad\quad\quad (2)\quad\quad\quad\quad\quad\quad\quad (3)$$

(1) Soil emission attenuated by the vegetation

(2) Vegetation emission

(3) Vegetation emission reflected by the soil

(b) Active microwave

$$\sigma = \gamma^2\sigma_{soil} + \sigma_{veg} \quad \text{where} \quad \sigma_{veg} = (1-\gamma^2)A\cos\theta$$
$$\quad (1)\quad\quad\quad\quad\quad\quad\quad\quad\quad (2)$$

(1) Signal scattered by the soil and attenuated by the vegetation

(2) Signal scattered by the vegetation
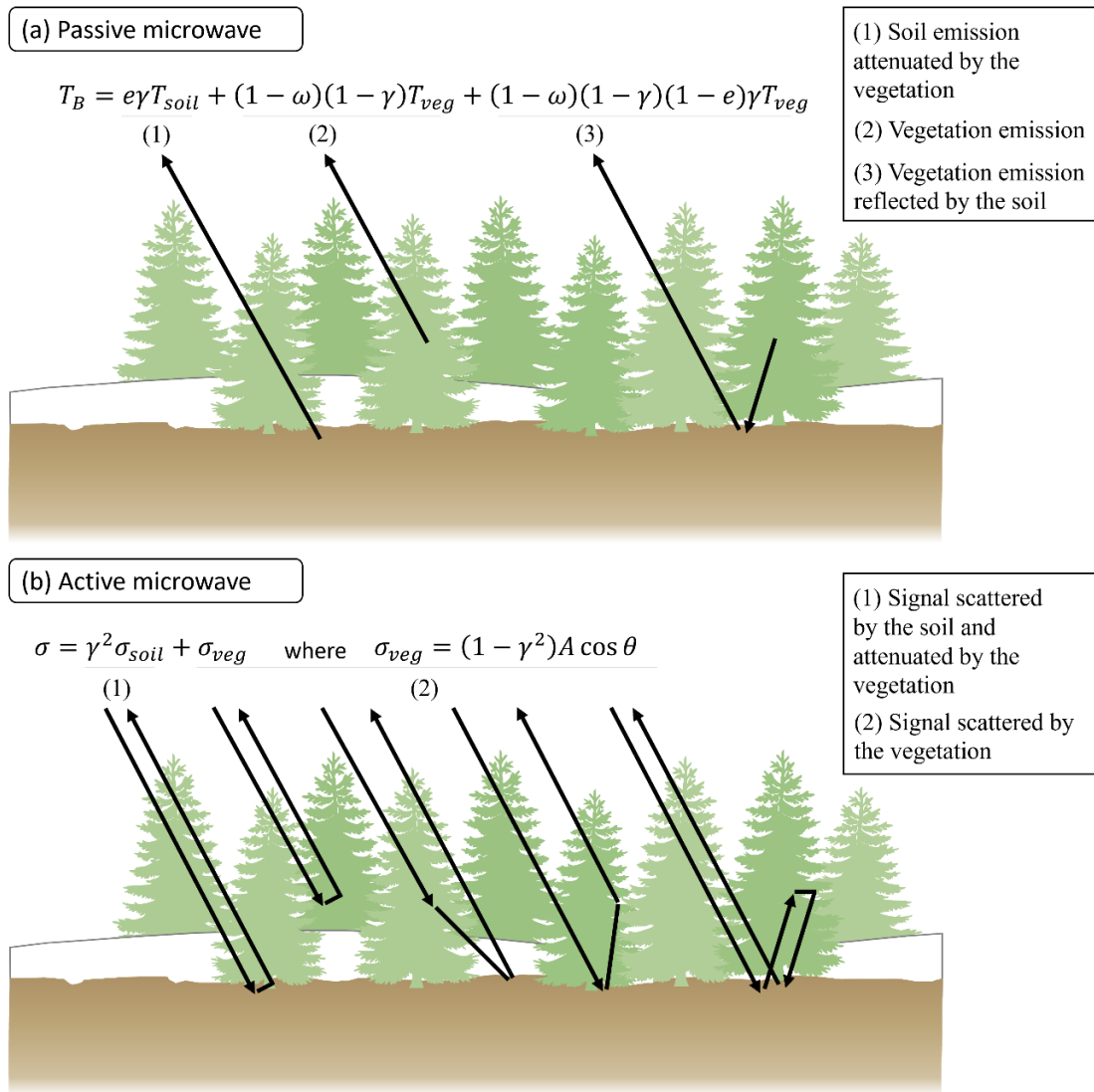
Figure 2: Microwave signal decoupling through electromagnetic wave interaction with matter. (a) Mo et al., (1982) model for passive microwave with T_B representing the brightness temperature, e the soil emissivity, γ the vegetation attenuation, ω the vegetation single-scattering albedo, and T the thermodynamic temperature of soil and vegetation (Mo et al., 1982). (b) water cloud model for active microwave with σ representing the backscattering coefficient, γ vegetation attenuation, A is a vegetation empirical parameter and θ the radar incident angle (Attema and Ulaby, 1978). The σ_{veg} term is an approximation for the first-order vegetation scattering processes. Snow increases the complexity of the interaction between the microwave and the ground level because it is acting as an additional semi-opaque layer comparable to the vegetation layer. Snow and atmosphere are not accounted for in the equations presented.

Multiple microwave radiometers have been launched in recent decades covering most of the microwave
portion of the electromagnetic spectrum: L-band (1-2 GHz), C-band (4-8 GHz), X-band (8-12 GHz), K-band
(18-26.5 GHz), K_a-band (26.5-40 GHz) and W-band (75-110 GHz) (Table A1). There is a nearly continuous
publicly available radiometric dataset from 1978 to the present covering the microwave bands from C-band
to W-band (Fig. 3a). Additionally, in the last decade, L-band data have become accessible through the launch
of the Soil Moisture Ocean Salinity mission (SMOS; Kerr et al., 2010), the Aquarius mission (Brucker et al.,
2004) and the NASA (National Aeronautics and Space Administration) Soil Moisture Active Passive mission
(SMAP; Entekhabi et al., 2010). An exhaustive list of radars would be too long to present here; instead we
focus on a selection of recent radar missions (Fig. 3b). These spaceborne radars were selected for the purpose
of the review to represent a range of frequencies and available temporal coverage.
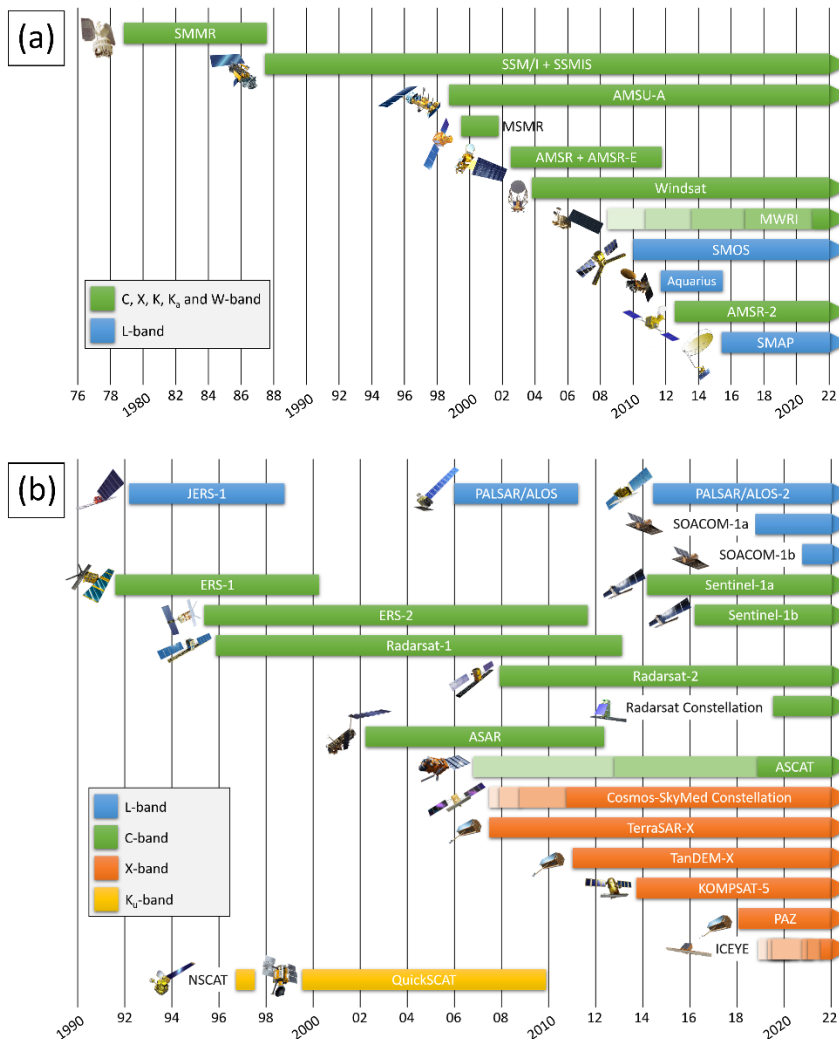
200

Figure 3: a) Temporal coverage of spaceborne passive microwave instruments (radiometers between 1-100 GHz, sun-synchronous nearly polar orbits, more details in Table A1). b) Selected number of spaceborne radar missions (active sensors) covering the L-band (1-2 GHz), C-band (4-8 GHz), X-band (8-12 GHz) and K_u-band (12-18 GHz). More details are provided in Table A2.

 3 Microwave remote sensing for retrieval of surface variables

Although direct measurements of vertical C fluxes are not feasible through microwave remote sensing, it is possible to use spaceborne radiometers and radar to monitor key variables important for different C cycle processes (Fig. 4). Carbon dioxide and CH_4 fluxes, two of the most potent greenhouse gases, are continuously exchanged between the Earth's surface and the atmosphere. Carbon dioxide is absorbed through photosynthesis by vegetation and is released by plants and soil through respiration (i.e., autotrophic respiration, R_a, and heterotrophic respiration, R_h, respectively) (Chapin et al., 2006). In ecosystems, CH_4 is produced by methanogens under anaerobic conditions and consumed during oxidation by methanotrophs under aerobic conditions (Lai, 2009). Methane transport through the soil column and to the atmosphere occurs through diffusion, ebullition, and plant-mediated transport (Lai, 2009).
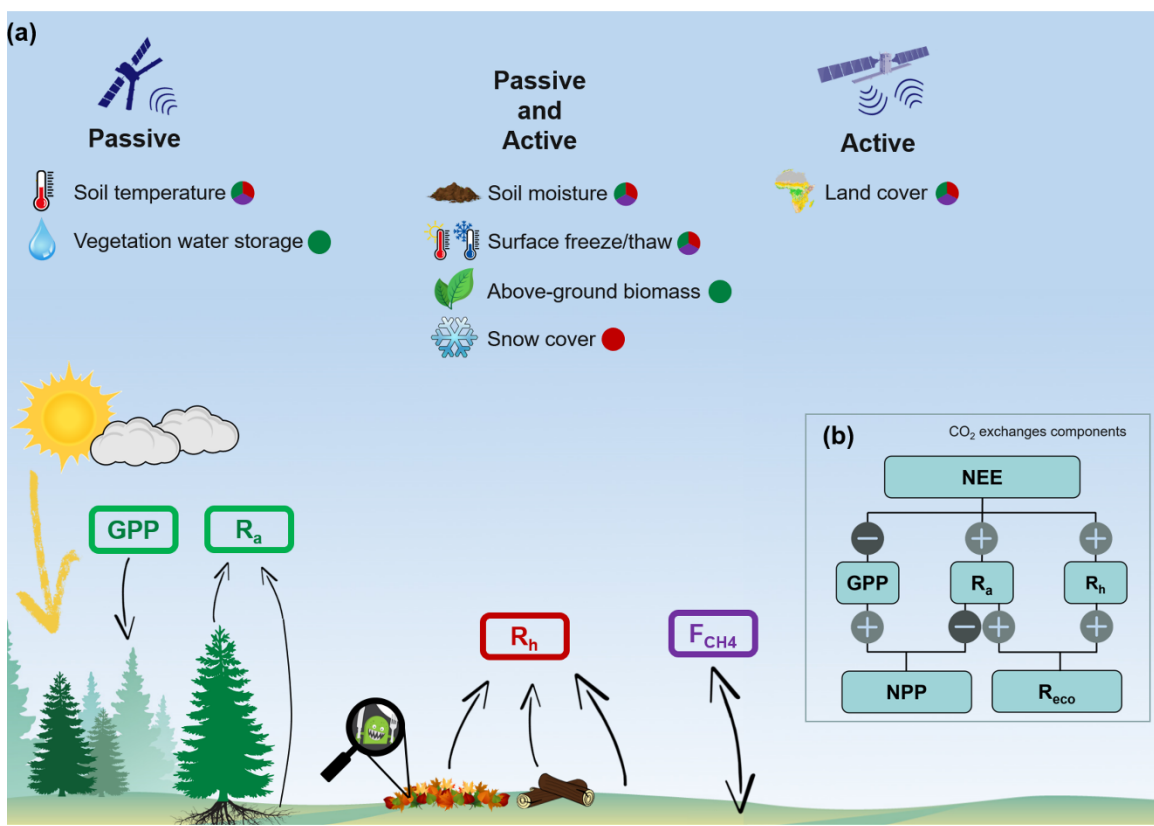
Figure 4: a) Carbon dioxide and methane fluxes between the land surface and the atmosphere including gross primary production (GPP), heterotrophic respiration (R_h), autotrophic respiration (R_a), and net methane fluxes (F_{CH4}) (units: gC m^{-2} yr^{-1}). The fluxes are color-coded (green: GPP and R_a; red: R_h; purple: F_{CH4}) to match which relevant key variables important for CO_2 and CH_4 fluxes and derivable with microwave remote sensing, and b) relationships of net primary productivity and net ecosystem productivity (NEP = - net ecosystem exchange [NEE]), and their component fluxes with ecosystem respiration [ER] = R_a + R_h.

3.1 Soil moisture

225   In the ABR, water availability, and air and soil temperatures are considered important environmental constraints on photosynthesis and thus C sequestration (Lieffers and Rothwell, 1987; Angert et al., 2005; Jones et al., 2017). For example, both heat stress and drought can limit tree growth across latitudes in boreal forest stands (Walker et Johnstone, 2014; Sniderhan et al., 2021). Near-surface soil moisture also affects methanogenesis and methanotrophy, which depends strongly on oxygen availability (Lai, 2009).

230 Environmental controls on soil respiration, i.e., the sum of belowground R_a and R_h, include soil moisture and temperature, which in the ABR are both influenced by permafrost and active (seasonally thawed) layer dynamics (Huntzinger et al., 2020). Hence, in a changing climate where soils across the ABR are generally expected to be drying (e.g., Gauthier et al., 2015; Andresen et al., 2020), reliably quantifying soil moisture dynamics and thus water availability will become essential for a predictive understanding of C cycle

235 dynamics.

     The sensitivity of the microwave signal to soil moisture content has been widely demonstrated previously but several challenges remain including accounting for vegetation attenuation and scattering related to the surface roughness (Das and Paul, 2015; Colliander et al., 2022), as well as organic soil model parametrization

240 (Mironov and Savin, 2015; Bircher et al., 2016). The sensitivity to soil moisture generally increases with lower microwave frequencies, making L-band the most sensitive to soil moisture content. The depth over which soil moisture content can be estimated from microwave remote sensing is limited at best to the top 5 cm of the soil profile (roots are most dense in the top 20 cm). Measurement depth depends on the frequency used (longer wavelengths realize greater depths; Adams et al. 2015), the soil moisture content and the

245 vegetation type and density (Wigneron et al. 2007). These measurement depths do not capture the water availability in the full rooting zone, which will be most relevant to predicting photosynthetic CO_2 update. However, it remains possible to estimate root zone soil moisture content from near-surface soil moisture content using pedotransfer equations meaning these surface measurements can be quite useful (Stefan et al., 2021; Dimitrov et al., 2022).

250

     Extensive methodological research to develop soil moisture retrievals from microwave remote sensing has been motivated for agricultural applications (Engman, 1991; Wigneron et al., 2007; Lakhankar et al., 2009). Soil moisture retrieval was the main motivation behind several passive L-band satellite missions, including SMAP and SMOS. The resulting expertise and soil moisture products present a promising data

255 stream to inform terrestrial biosphere models (see sect 4). Table 1 presents several soil moisture products available. The European Space Agency (ESA) Climate Change Initiative (CCI) project produces a soil moisture product merging active and passive microwave sensors exploiting the microwave instruments temporal coverage since 1978 (Gruber et al., 2019).

260

Table 1: Presently available soil moisture products from spaceborne microwave remote sensing.

	Windsat[1]	SMOS[2]	Aquarius[3]	AMSR-E/2[4]	SMAP[5]	ERS 1-2[6]	ASCAT[7]	RADARSAT-2[8]	Sentinel-1 A/B[9]	Climate Change Initiative[10]
Sensor type	Passive	Passive	Passive	Passive	Passive	Active	Active	Active	Active	Passive and Active
Spatial Resolution	25 km	25 km	36 km	25 km	9 km	25 km	25 km	18 m	1 km	25 km
Temporal coverage	2003-2012	2010-ongoing	2011-2015	2002-ongoing	2015-ongoing	1996-2011	2007-ongoing	2007-ongoing	2015-ongoing	1978-ongoing
Reference	Parinussa et al., 2012	Al Bitar et al., 2017	Bindlish et al., 2015	Du et al., 2017	Chan et al., 2016 and 2018	Naeimi et al., 2009; Das et al., 2017	Wagner et al., 2013	Merzouki et al., 2011	El Hajj et al., 2017	Gruber et al., 2019

[1]WindSat/Coriolis surface soil moisture (LPRM) L3 1 day 25 km x 25 km daytime V001
[2]SMOS L1 and L2 Science data
[3]Aquarius L3 Weekly Polar-Gridded Sea Surface Salinity, Version 5 (AQ3_SSS)
[4]AMSR-E/AMSR2 Unified L2B Half-Orbit 25 km EASE-Grid Surface Soil Moisture, Version 1 (AU_Land)
[5]SMAP L4 Global 3-hourly 9 km EASE-Grid Surface and Root Zone Soil Moisture Geophysical Data, Version 6 (SPL4SMGP)
[6]ERS-2 SCATTEROMETER Surface Soil Moisture Time Series and Orbit product in High and Nominal Resolution
[7]ASCAT Soil Moisture at 25 km Swath Grid in NRT - Metop
[8]RADARSAT-2 Surface Soil Moisture
[9]1km SSM Version 1 product (SSM1km)
[10]ESA CCI SM

3.2 Soil temperature

265   Rates of photosynthesis and ecosystem respiration (R_{eco}; Fig. 4) are generally strongly controlled by soil temperature (Anger et al., 2005; Jones et al., 2017; Stocker et al., 2018). Similarly, laboratory and field observations have shown that R_h-related CO_2 fluxes are non-negligible below freezing point and increase with warming soil temperatures (Fahnestock et al., 1998 and 1999; Welker et al., 2000; Mikan et al., 2002; Panikov et al., 2006; Natali et al. 2019). Despite lower fluxes, winter CO_2 emissions from soil respiration may constitute an important contribution to annual net ecosystem productivity (NEP), especially in ABR with very short growing seasons (Elberling et al., 2007; Webb et al., 2016; Natali et al., 2019).

Microwave T_B depends on thermodynamic temperature ($T_B = e \cdot T$), thus it is possible to retrieve land surface temperature (LST) from radiometric data (Duan et al., 2020). Retrieval of LST from microwave remote sensing is technically more challenging and results in lower precision than similar products from thermal infrared remote sensing, 1-5 K for microwave LST vs. 0.2-2K for thermal infrared (Jiménez-Muñoz and Sobrino, 2006; Jones et al., 2010; Osińska-Skotak, 2007; Krishnan et al., 2020; Zhang and Cheng, 2020). Microwave emissivity is also more sensitive to environmental changes (e.g., liquid water content) than thermal infrared emissivity. Although infrared LST is more precise than microwave LST, there are instances where microwave LST may be important. Specifically, microwave LST can support gap-filling when thermal infrared LST is unavailable because of extended periods of cloud cover or when fine temporal resolution is required. Microwave can be used to sense soil temperature up to a few centimeters deep because of its soil penetration depth. It is an important advantage over thermal infrared remote sensing, which can only detect LST and is subject to significant atmospheric contamination (Jones et al., 2007). Some studies have also shown the potential to use microwave observations to retrieve soil temperature under the snow (Kohn et al., 2010; Marchand et al., 2018).

Although several studies have obtained LST from microwave data, no operational microwave LST product is operationally available. Microwave LST algorithms typically achieve a precision of 2-5 K using data from AMSR-E/2 (Jones et al., 2010; Zhang and Cheng, 2020) and SMM/I-SMMR (Pulliainen et al., 1997; Basist et al., 1998; Fily et al.; 2003; Mialon et al., 2007; Royer and Poirier, 2010). Other studies have used machine learning approaches, obtaining precision around 1-3 K with AMSR-2 data (Aires et al., 2001; Mao et al., 2018).

3.3 Surface freeze/thaw state

During the short growing season in the ABR, photosynthetic CO_2 uptake exceeds the respiratory CO_2 losses, thus ABR generally act as net growing season CO_2 sinks (Ciais et al., 2019; Virkkala et al.; 2021). However, in winter, plants become dormant and photosynthesis and R_a cease (gross primary productivity, GPP = 0 and $R_a \approx 0$) owing to the cold temperatures and highly reduced photoperiod (Kimball et al., 2004b; Rafat et al. 2021). Although R_h may continue in frozen soil, it decreases substantially (Natali et al., 2019). Modelling annual NEP in areas undergoing seasonal surface freeze/thaw cycles requires the ability to estimate the length and timing of the growing season (Seiler et al., 2022; El-Amine et al., 2022). Growing season length has a direct impact on annual GPP and thus NEP but there is also a strong relationship between surface freeze/thaw timing and photosynthetic CO_2 uptake (Frolking et al., 1996; McDonald et al., 2004; Kim et al. 2012; Fu et al., 2017; Pierrat et al., 2021). Changes in the timing of spring thaw can create a shift in growing conditions when photosynthesis is initiated (Jarvis and Linder, 2000; Tanja et al., 2003; Kimball et al., 2004a; Piao et al., 2008; Kim et al., 2012; El-Amine et al., 2022). The timing of the start of the growing season has been shown to be more important to annual GPP than the timing of the end because of the superior light and water availability during the spring period (Tanja et al., 2003; El-Amine et al., 2022). The surface freeze/thaw state is a useful proxy for the timing and thus duration of photosynthetic activity (Harrison et al., 2020), and can potentially be used to track CH_4 emissions in the ABR (Tenkanen et al., 2021).

Satellite detection of surface freeze/thaw state is based on the dielectric contrast between water and ice at microwave frequencies. Therefore, soil emissivity is highly sensitive to phase state changes of its liquid content. When water freezes, ε_{soil} drops drastically as liquid water changes to ice because of the crystalline structure of frozen water. The rapid decrease of ε_{soil} in freezing soils translates into a much higher microwave emission and backscattering from the surface. This allows for surface freeze/thaw state retrieval from passive and active microwave measurements using temporal change detection algorithms (Mortin et al., 2012; Rautiainen et al. 2012; Roy et al., 2015; Chen, et al., 2019) and threshold-based methods (Kim et al., 2012 and 2017; Derksen et al., 2017). Furthermore, for oblique incidence angles, horizontal polarization is more affected than its vertical counterpart during surface freeze/thaw transition which favors the use of a polarization ratio as an effective tool for determining surface freeze/thaw state (Rautiainen et al., 2016; Roy et al., 2017a and 2017b).

The use of passive and active microwave remote sensing for surface freeze/thaw state detection has been widely studied, improving quickly and steadily in the last decade, and resulting in various publicly available products (Table 2). As for soil moisture studies, lower microwave frequencies such as L-band, have been the most exploited because of the prominent water phase dielectric contrast and reduced attenuation from above-ground vegetation and snow (Rautiainen et al., 2014). Surface freeze/thaw state products offer the opportunity to constrain vegetation growing season timing and photosynthetic CO_2 uptake in terrestrial biosphere models.

Table 2: Available Surface freeze/thaw state products from spaceborne microwave remote sensing.

	MEaSUREs program[1]	Aquarius[2]	SMOS[3]	SMAP[4]	NSCAT	QuickSCAT	PALSAR	ASCAT[5]
Sensor type	Passive	Passive	Passive	Passive	Active	Active	Active	Active
Spatial Resolution	25 km (6 km starting in 2002)	36 km	25 km	9 km	25 km	25 km	5-500 m	25 km
Temporal coverage	1979-2020	2011-2015	2010-ongoing	2015-ongoing	1996-1997	1999-2009	2006-2011	2007-2021
Reference	Kawanishi et al., 2003	Xu et al., 2016; Prince et al., 2018	Rautiainen et al., 2016	Kim et al., 2019	Kimball et al., 2001	Brucker et al., 2014	Kerr et al., 2010	Naeimi et al., 2012

[1]Sensors: SMMR, SSM/I, SSMIS, AMSR-E and AMSR-2
[2]Aquarius L3 Weekly Polar-Gridded Landscape Freeze/Thaw Data, Version 5 (AQ3_FT)
[3]SMOS Level 3 Freeze and Thaw (F/T)
[4]SMAP Enhanced L3 Radiometer Global and Northern Hemisphere Daily 9 km EASE-Grid Freeze/Thaw State, Version 3 (SPL3FTP_E)
[5]ASCAT Surface Soil Moisture/Freeze-Thaw V2 product

3.4 Above-ground biomass

Although not a direct control on C cycle processes, aboveground biomass (AGB) can be used to estimate aboveground C stocks. The annual net gain or loss of C by vegetation (NPP) leads to a proportional increase or decrease in AGB, respectively (Turner et al., 2004; Gough, 2011). Therefore, C storage in aboveground vegetation over a defined period can be inferred from AGB estimates from either terrestrial, aerial, or spaceborne techniques (Das et al., 2021). However, using AGB only provides average C exchanges between two data acquisitions and provides no understanding of the underlying ecophysiological and biogeochemical processes. It should be noted that AGB is a minor component of the C stocks in ABR where most of the C is stored belowground (Houghton, 2005; Pappas et al., 2020; Walker et al., 2020). Information on AGB allows initialization, parameterization and evaluation of terrestrial biosphere models and helps to understand, for example, the impact of discrete disturbances such as wildfire and insect outbreaks (Chirici et al., 2016).

Microwave remote sensing can provide information on AGB since microwave wavelengths typically penetrate and interact with moderately dense vegetation cover, depending on the microwave length (Liu et al., 2011a, 2011b and 2015). Vegetation attenuation of microwaves is characterized by the vegetation optical depth (VOD; $\gamma = e^{-VOD/\cos\theta}$) which is proportional to vegetation density (i.e., biomass) and water content. Vegetation optical depth is frequency-dependent and affected by the geometry (e.g., canopy structure) of the vegetation (Ulaby et al., 1990). The impact of vegetation geometry on attenuation is challenging to

parametrize because of the complexity of forest canopies, therefore it is typically accounted for through vegetation type-dependent, empirically determined parameters introduced in the relationship between VOD, vegetation water content and biomass (Jackson and Schmugge, 1991; Konings et al. 2019). Microwave VOD is better suited to directly monitor vegetation compared to spectral vegetation indices obtained using visible
355 and infrared wavelengths such as NDVI that saturate at relatively low AGB of around 50-80 Mg ha^{-1} (Rodríguez-Fernández et al., 2018; Mialon et al. 2020; Turner et al., 2004). In contrast, VOD was shown to saturate at AGB of up to 350 Mg ha^{-1} (Vittucci et al., 2019). It has also been shown that there is a significative difference in what phenological aspects of the growing season are captured by vegetation indices such as NDVI versus microwave VOD (Milaon et al., 2020). VOD seems to correspond better to key physiological
360 processes such as sap flow and vegetation water storage than vegetation indices such as NDVI, which better capture dynamics of canopy phenology (Lawrence et al., 2014; Cui et al., 2015; Tian et al. 2016; Holtzman et al. 2021; Wigneron et al., 2021).

There is clear potential to improve C cycle science in boreal forests using VOD-derived AGB
365 (Rodríguez-Fernández et al., 2018). Several recent studies have also shown good correlations between VOD and GPP (Teubner et al., 2018 and 2019). The L-band spaceborne radiometer record goes back to 2010 with SMOS, while higher frequency VOD estimates extend back to the early 1980s. Table 3 presents several VOD products available. Santoro and Cartus (2018) counted 221 studies on SAR data applied to AGB retrieval from 1987 to 2017 using frequencies from 30 MHz up to 12 GHz. AGB investigations using active sensors
370 can achieve a much finer spatial resolution than their passive counterparts, down to the 10 m scale. Also, recent promising advances in SAR interferometry (InSAR), polarimetric InSAR (PolInSAR) and SAR tomography (TomoSAR) techniques provide new opportunities for AGB estimates by surveying the 3D structure of vegetation (Neumann et al., 2012; Tebaldini et al., 2019). InSAR can be used to measure the vertical motion in peatlands which is a direct indicator of the mass gain or loss by those ecosystems which
375 constitute a major global C pool (Alshammari et al., 2019; Zhou et al., 2019; Loisel et al. 2021). Some global biomass surveys have also exploited the multi-frequency synergy of data products in the microwave, visible and infrared wavelengths, and LiDAR technologies (e.g., GlobBiomass: Santoro et al., 2018; Mialon et al., 2020). Although the low AGB of the Arctic tundra is challenging to monitor from microwave observations, studies have shown that it is possible to estimate the upper soil organic C (up to 30 cm from the
380 soil/atmosphere interface) using active and passive microwave observations (Bartsch et al. 2016; Yi et al. 2022).

385

Table 3: Available vegetation optical depth products from spaceborne microwave remote sensing.

	AMSR-E/2[1]	SMOS[2]	SMAP	221 SAR studies	ASCAT
Sensor type	Passive	Passive	Passive	Active	Active
Spatial Resolution	25 km	25 km	36 km	>= 10m	25 km
Temporal coverage	2002-2020	2010-ongoing	2015-ongoing	1987-2017	2015-2019
Reference	Jones et al., 2011; Du et al., 2017	Wigneron et al., 2021	Li et al., 2022	Santoro and Cartus, 2018	Liu et al., 2021

[1]Daily Global Land Parameters Derived from AMSR-E and AMSR2, Version 3 (NSIDC-0451)
[2]L3 SMOS IC L-VOD VERSION 2
[3]SMAP-IB L-VOD
[4]ASCAT-IB VOD

3.5 Vegetation water storage

Water availability is considered an important environmental limitation on photosynthetic processes in the ABR (Ruiz-Pérez et Vico, 2020). In terrestrial biosphere models, lack of water availability is an environmental stress reducing the photosynthetic capacity (i.e., NPP) (Mu et al., 2007). Water stored in vegetation is critical for stomatal regulation, therefore it is strongly correlated to vegetation growth (Kocher et al. 2013; Matheny et al., 2015). In addition, vegetation water storage can act as a buffer for the daily demands of transpiration (Matheny et al., 2015). However, soil moisture and/or precipitation are generally used to estimate water availability since vegetation water storage estimates are rarely available (Zhang et al., 2015; Stocker et al., 2018).

Since vegetation water storage strongly affects microwave VOD because of the high absorption of microwave by water (Konings et al., 2019), microwave attenuation holds potential for estimating vegetation water storage, which can be used to evaluate vegetation water stress (Holtzman et al., 2021). To the best of our knowledge, no large-scale vegetation water storage product yet exists, but efforts toward this goal are underway (Liu et al., 2021). The microwave VOD sensitivity to both AGB and vegetation water status complicates its interpretation, although the study of the temporal and spatial trends of VOD can allow to distangle AGB vs the vegetation water content (Dou et al., 2023). At short timescales (i.e., diurnal), biomass variation is small and VOD trends can largely be attributed to vegetation water status. At longer timescales (i.e., annual), VOD trends come mostly from biomass dynamics (Mialon et al., 2020). Another method to distinguish water storage and biomass related VOD changes is to use periods with similar water stress levels for VOD comparison (Konings et al., 2019).

3.6 Land cover

Regional and global studies on C exchanges require information on land cover (Gasser et al., 2020). Repeated satellite-based image classification provides large scale monitoring of land cover evolution (Wang et al., 2019). Land cover and wetland classifications based on SAR imagery have been developed with the same supervised or unsupervised classification algorithms used for classifying imagery obtained with visible and infrared remote sensing (van Zyl, 1989; Pierce et al., 1994; Dobson et al., 1995; Ranson and Sun, 2000; Bartsch et al., 2007; Witcomb et al., 2009; Lönnqvist et al., 2010; Merchant et al., 2017; Merchant et al., 2022). Recent studies have explored the use of machine learning for land cover classification based on SAR data (Merchant et al., 2019). SAR land cover classifications are enhanced when benefiting from multi-frequency instruments (Saatchi and Rignot; 1997) and multiple polarizations (Lee et al., 2001). The complementarity of SAR and visible/infrared imagery has already been exploited to reinforce spatial and temporal coverage and improve precision of land cover classifications (Töyrä et al., 2001; Ulman et al., 2014; Merchant et al., 2019). SAR imagery has shown to be especially useful for delineating inundated areas (Bowling et al., 2003) or wet and moist tundra (Morrissey et al., 1996; Merchant et al., 2022) which has a strong impact on CH4 emission (Watts et al., 2014). Microwave observations can also be used to monitor freshwater bodies (FW) extent dynamics (Murfitt and Duguay, 2021). FW can act as important CH_4 emissions sources, especially during ice melt but aquatic carbon cycle processes are much different than terrestrial carbon processes and were not within of the scope of this review (Matthews et al., 2020).

3.7 Snow cover

Unlike photosynthesis and R_a, R_h can continue through winter in the cold regions. The insulating properties of snow cover have an important indirect impact on C fluxes, keeping the ground warmer than the air during winter thereby maintaining microbial activity and therefore R_h (Brooks et al., 1997; Brooks and Williams, 1999; Welker et al., 2000; Elberling et al., 2007; Ravn et al., 2020). Through modelling the land surface energy exchanges, the impact of snow on the soil thermal regime can be estimated (Melton et al., 2020). Several studies have demonstrated a correlation between C fluxes and snow depth due to the insulating properties of snow (Björkman et al., 2010; Rogers et al., 2010; Natali et al., 2019). Furthermore, snow density is the main factor controlling snow thermal conductivity (Sturm et al., 1997), which should consequently influence soil temperature, winter CO_2 and CH_4 fluxes.

Estimating snow accumulation in the ABR represents a challenge for microwave remote sensing. Microwaves are partially absorbed and scattered by snow cover, with an additional challenge in the boreal forest because of snow interception by the forest canopy (Li et al., 2019). Active and passive microwaves can retrieve information about the snowpack status based on microwave interaction with the snow microstructure (Picard et al., 2018). Because multiple snowpack characteristics influence microwaves in many ways (i.e., height, density, microstructure, layering, liquid water content), retrieving snowpack characteristics often leads to an underdetermined equation system (i.e., fewer equations than unknowns).

During springtime and winter rain-on-snow events, wet snow becomes a major limitation for microwave remote sensing. Liquid water absorbs microwave radiation, reducing microwave penetration depth in wet snow and preventing acquisition of information about either the snow or the underlying ground conditions. This is especially problematic for the retrieval of surface freeze/thaw state during the spring thaw (Rautiainen et al., 2016). However, snowmelt is easily detected (Forster et al., 2001) and can serve as a proxy for the beginning of the growing season, and the resulting initiation of C uptake (Pulliainen et al., 2017).

Estimating the snow water equivalent (SWE, i.e., the product of snow depth and density) is widely used to monitor bulk snow cover using microwaves (Chang et al., 1982; Pulliainen, 2006; Shi et al., 2016; Pulliainen et al., 2020; Saberi et al., 2020). It should be noted that uncertainties are higher in the presence of vegetation because of the ensuing microwave attenuation (Mortimer et al., 2020) and for deep snow conditions (SWE > 150 mm: Larue et al., 2017).

Table 4: Available snow water equivalent (SWE) products from spaceborne microwave remote sensing.

	GlobSnow[2]	AMSR-E/2[1]
Sensor type	Passive	Passive
Spatial Resolution	25 km	25 km
Temporal coverage	1980-2018	2002-ongoing
Reference	Luojus et al., 2021	Tedesco and Jeyaratnam, 2016

[1]AMSR-E/AMSR2 Unified L3 Global Daily 25 km EASE-Grid Snow Water Equivalent, Version 1 (AU_DySno)
[2]GlobSnow v3.0 NH SWE; Sensors: SMMR, SSM/I, SSMIS
se

4 Assimilating microwave data in terrestrial biosphere models in Arctic-boreal regions

Microwave remote sensing has the potential to greatly improve predictions of C fluxes in terrestrial biosphere models. However, the use of key variables obtained from microwave remote sensing to inform terrestrial biosphere models is still limited (Lees et al., 2018). A recent effort assimilates a microwave remote sensing soil moisture data product into a simple C cycle model to compute the SMAP L4 global daily 9km EASE-Grid carbon net ecosystem exchange product (SPL4CMDL, Jones et al., 2017; Fig. 5).. The SPL4CMDL product provides daily NEE, GPP, R_h, soil organic C, and environmental constraints for eight plant functional types at 9 km spatial resolution. The product is publicly available with data starting in 2015. The L4C carbon exchange model estimates GPP using a light use efficiency model, R_a is defined as a fraction of GPP and R_h is estimated using a soil decomposition model with cascading soil organic C. The GEOS-5 atmospheric model is used for the meteorological inputs and MODIS visible/infrared products is used for

land cover and photosynthetically active radiation. There is ongoing work to improve L4C estimates by
integrating surface freeze/thaw state information from microwave remote sensing. The SMAP L4C product
is currently the only operational C exchange model using satellite microwave information, which provides
direct information for studying seasonal cycles and long-term trends in ecosystem C exchange (Fig. 6).
SMOS soil moisture data has similarly been used in terrestrial biosphere models but for a shorter period
(2010-2015; Wu et al. 2020). Lastly, the terrestrial C flux (TCF; Kimball et al., 2009) model used AMSR-E
soil moisture and temperature information to provide environmental constraints on R_h in Arctic-boreal
regions (Baldocchi et al., 2001; Pastorello et al., 2020). Although limited so far, those examples show the
potential of integrating microwave products in terrestrial biosphere models.
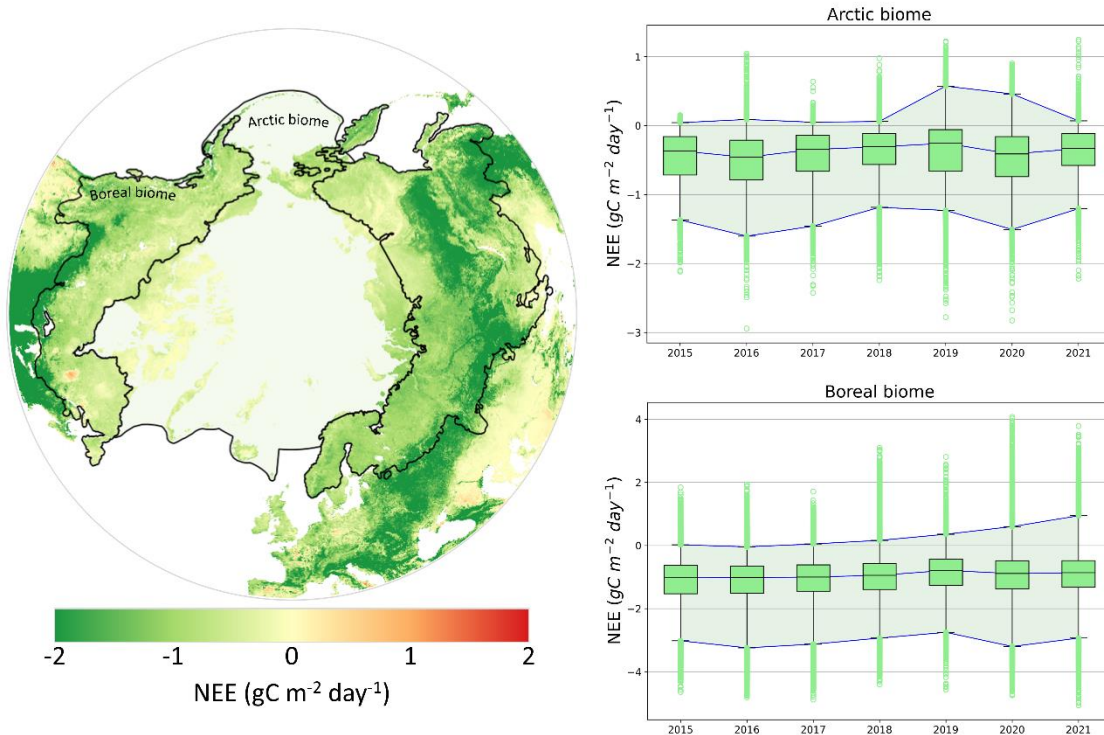
Figure 5: Mean monthly net ecosystem exchange (NEE) from the SPL4CMDL for July and August (i.e., peak growing season) between 2015 and 2021. The Arctic biome is delimited following the Conservation of Arctic Flora and Fauna (CAFF) working group of the Arctic Council and the boreal biome is delineated following Potapov et al. (2008). The yearly mean NEE for the Arctic- ($N_{pixel} = 282\ 288$) and boreal regions ($N_{pixel} = 187\ 003$) is presented as boxplots for the 25-75 percentiles (box) and the 1-99 percentiles (bracket). SMAP L4C reference: Kimball et al. (2017).

5 Challenges and opportunities in microwave remote sensing for supporting carbon cycle science

Although microwave remote sensing data processing is reaching a certain maturity after decades of development, challenges remain in the advancement of microwave data and their assimilation into terrestrial biosphere models (Jones et al., 2017).

5.1 Disentangling the integrated microwave signal

495   Disentangling the integrated microwave signal originating from varying mixtures of soil, vegetation and snow remains challenging for all microwave remote sensing applications (Kerr et al., 2012; Roy et al., 2012 and 2014). Recent advances have been made for both passive and active data to decouple the signal in boreal forests by exploiting multi-polarization, multi-angular and multi-frequency measurements (Larue et al., 2018; Cohen et al., 2019; Konings et al., 2019; Roy et al., 2020). Even in the Arctic biome where AGB

500   is relatively low, the plot-scale heterogeneity in vegetation composition and structure can pose a challenge since repeated field estimates of vegetation distribution are limited (Myers-Smith et al., 2011; Du et al., 2019). Furthermore, the low C fluxes of the ABR can be more challenging to estimate, and vegetation production trends can be lost in interannual variability fluctuations (i.e., low signal:noise ratio). The decoupling challenge can be exemplified clearly with the respective effects of soil and vegetation on surface

505   freeze/thaw state detection since soil and vegetation might not freeze or thaw concurrently with implications for detection of surface freeze/thaw events (Roy et al., 2020). Microwave data processing must account for the high density of shallow water bodies in ABR, and recent efforts have sought to remove their effect on passive microwave observations mixed pixels (Touati et al., 2019). These challenges highlight the importance of continued efforts to improve radiative transfer modelling in a way that will allow for the decoupling the

510   contribution of different components to the microwave signal.

5.2 Intra-pixel variability

        Due to the coarse spatial resolution of passive microwave data products, intra-pixel variability and downscaling are important considerations. For exemple, a recent study from Prince et al. (2019) upholds that

515   the time span of the surface freeze/thaw signal transition in passive microwave measurements might be related to the spatial variability of the soil state (frozen or thawed) through this transition (i.e., patchy frozen soil). Intra-pixel variability also includes partial presence of snow during transition seasons, vegetation types mixing and snow depth distribution (Meloche et al., 2022). A recent study from Du et al. (2020) showed promising results in downscaling soil moisture to 3 m spatial resolution using machine-learning with

520   microwave spaceborne data. Although challenging for sub-regional studies, the typical passive microwave remote sensing spatial resolution is well suited for regional and global climate studies. Still, most of the terrestrial biosphere model performance evaluation is done using eddy covariance data which is the most trusted and widely used reference for C flux measurements at large scales. However, the sparsity of the measurement network in ABR reduce our capacity to represent ABR heterogeneity in terrestrial biosphere

525   model (Fig. 1; Fisher et al., 2018). However, the scale mismatch between measurements is important to keep in mind; tower-based measurements of C exchanges represent footprints of approximately 1 km or less, which is a much smaller scale than many spaceborne microwave remote sensing data products.

5.3 Potential and upcoming spaceborne microwave remote sensing missions

530   Upcoming spaceborne microwave remote sensing missions will provide new microwave sensors with additional frequencies and generally improved radiometric and spatial resolution (Table 5). These upcoming missions will increase remote sensing capabilities and extend the continuous microwave coverage over the next decade. The technical and scientific advances made through these missions should be seen as an additional motivation to actively identify ways to integrate microwave data products in C cycle science.

535   Furthermore, the novel approach of opportunistic use of spaceborne reflectometry of the Global Navigation Satellite System (GNSS) (Li et al., 2022; Yu et al., 2022) already showed promising results in evaluating soil moisture (Edokossi et al., 2020), soil freeze/thaw state (Rautiainen et al., 2021) and snow water equivalent (Royer et al. 2021).

540   **Table 5:** Overview of selected future microwave satellite missions with a polar or near-polar orbit.

Mission	SMOS-HR	CIMR	BIOMASS	NISAR	Tandem-L	ROSE-L
Space agency	CNES	ESA (Copernicus program)	ESA	NASA and ISRO	DLR	ESA (Copernicus program)
Frequency (GHz)	L-band	1.4, 6.9, 10.65, 18.7 and 36.5	P-band	L- and P-band	X-band	L-band
Sensor type	Radiometer	Radiometer	SAR	SAR	SAR constellation	SAR
Spatial resolution expected	10 km	5 – 55 km	200 m	3 – 10 m	7 – 100 m	5 – 10 m
Revisit coverage expected (days)	N/A	N/A	25-45	12	16	3-6
Main objective	SMOS continuity	AMSR continuity	Biomass	Land elevation (including biomass)	Biomass, soil moisture and permafrost	SWE, soil moisture and permafrost
Expected launch	Development phase	Development phase	2022	2022	2022	Development phase
References	Rodríguez-Fernández et al., 2019a and 2019b	Kilic et al., 2019	Le Toan et al., 2011; Schlund et al., 2018; Quegan et al., 2019	Alvarez-Salazar et al., 2014; Rosen et al., 2015 and 2016; Kim et al., 2017	Bachmann et al., 2016; Huber et al., 2016; Krieger et al., 2016; Moreira et al., 2018	Pierdicca et al., 2019

6 Conclusions

Microwave remote sensing is an efficient tool for monitoring soil, seasonal snow and vegetation properties affecting water and C cycle processes and thus has great potential to enhance our understanding

545   of rapidly changing arctic-boreal regions. Understanding C cycle processes in arctic-boreal regions will greatly benefit from an increased use of microwave data which can only result from expanded collaboration between the microwave remote sensing and C cycle science communities. The potential applications of

satellite-based microwave remote sensing in support of C cycle science have not been fully realized. We propose four key aspects where increased use of microwave remote sensing could support advances in C

550 cycle science and monitoring: 1) Improve radiative transfer model skills and capabilities and the understanding of microwave signals associated with different surface material; 2) improve assimilation approaches of microwave products in terrestrial biosphere models to overcome the challenges associated with remote cold regions where ground observations are spatially and temporally sparse; 3) develop and maintain long-term, spatially-distributed, land-based measurement networks in arctic-boreal regions to improve

555 microwave-based products; 4) keep a long-term perspective and coherency between space agencies to maintain the historical trends of microwave observations.

7 Author contribution

AM, OS, and AR conceptualized the manuscript goal and objectives. AM prepared the manuscript with contributions from all co-authors.

560 **8 Competing interests**

The authors declare that they have no conflict of interest.

9 Acknowledgments

This work was made possible thanks to a PhD scholarship obtained from by the Natural Sciences and Engineering Research of Canada Council (NSERC), and funding obtained from the Fonds Québécois de

565 la Recherche sur la Nature et les Technologies (FQRNT) and the Canadian Space Agency (CSA).

570

575

10 Acronyms and abbreviations

ASAR	Advanced Synthetic Aperture Radar
ASCAT	Advanced SCATterometer
AGB	Above-Ground Biomass
AMSR	Advanced Microwave Scanning Radiometer
AMSR-E	AMSR for Earth Observing System
APAR	Absorbed Photosynthetically Active Radiation
CARDAMOM	Carbon data model framework
CCI	Climate Change Initiative
CIMR	Copernicus Imaging Microwave Radiometer
CLM	Community Land Model
CNES	Centre National d'Études Spatiales
CO_2	Carbone dioxide
CH_4	Methane
CSA	Canadian Space Agency
DLR	German Aerospace Center
e	Soil emissivity
ERS	European Remote sensingsatellites
ESA	European Space Agency
EVI	Enhanced Vegetation Index
FAO	Food and Agriculture Organization of the United Nations
FY-3	FenYun-3
FW	Freshwater
fPAR	Fraction of Photosynthetically Active Radiation
$f(x_i)$	General environmental stress function
GEOS-5	Goddard Earth Observing System, Version 5
GNSS	Global Navigation Satellite System
GPP	Gross Primary Production
H_2O	Water
IFOV	Instantaneous Field Of View
InSAR	SAR interferometry
ISRO	Indian Space Research Organisation
LAI	Leaf Area Index

LiDAR	Light Detection And Ranging
LPJ-wsl	Lund–Potsdam–Jena dynamic global vegetation model - Wald Schnee und Landscaft version
LST	Land Surface Temperature
MEaSUREs	Making Earth System data records for Use in Research Environments
MODIS	MODerate-resolution Imaging Spectroradiometer
MPI	Max Planck Institute
MWRI	Micro-Wave Radiation Imager
NASA	National Aeronautics and Space Administration
NDVI	Normalized difference vegetation index
NEE	Net Ecosystem Exchange
NEP	Net Ecosystem Production
NISAR	NASA-ISRO SAR mission
NPP	Net Primary Production
NSCAT	NASA Scatterometer
PALSAR	Phased Array type L-band SAR
PAR	Photosynthetically Active Radiation
PolInSAR	Polatrimetric InSAR
PRI	Photochemical Reflectance Index
QuickSCAT	Quick Scatterometer
R_a	Autotrophic respiration
R_{eco}	Ecosystem respiration
R_h	Heterotrophic respiration
REP	Red Edge Position
ROS	Rain-On-Snow events
ROSE-L	Radar Observing System for Europe - L-Band
SAR	Synthetic Aperture Radars
SMAP	Soil Moisture Active Passive
SMAP L4C	SMAP Level 4 Carbon product
SMMR	Scanning Multichannel Microwave Radiometer
SMOS	Soil Moisture and Ocean Salinity
SMOS-HR	SMOS High-Resolution
SMRT	Snow Microwave Radiative Transfer model
SWE	Snow Water Equivalent
SSM/I	Special Sensor Microwave/Imager

T_B	Brightness temperature
TCF	Terrestrial Carbon Flux
TomoSAR	SAR tomography
UNAVCO	University NAVstar COnsortium
VOD	Vegetation Optical Depth
γ	Vegetation attenuation
η	Light conversion efficiency
η_{max}	Light conversion efficiency maximum in optimal conditions
$\boldsymbol{\varepsilon}$	Relative permittivity
θ	Incident angle
σ	Backscattering coefficient
τ	Optical depth
Ω	Vegetation single-scattering albedo

11 References

Adams, J., McNairn, H., Berg, A., and Champagne, C.: Evaluation of near-surface soil moisture data from an AAFC monitoring network in Manitoba, Canada: implications for L-band satellite validation. J. Hydrol., 521, 582-592, doi: 10.1016/j.jhydrol.2014.10.024, 2015.

Aires, F., Prigent, C., Rossow, W., and Rothtein, M.: A new neural network approach including first guess for retrieval of atmospheric water vapor, cloud liquid water path, surface temperature, and emissivities over land from satellite microwave observations. J. Geophys. Res.-Atmos2., 106(D14), 14887-14907, doi: 10.1029/2001JD900085, 2001.

Al Bitar, A., Mialon, A., Kerr, Y. H., Cabot, F., Richaume, P., Jacquette, E., Quesney, A., Mahmoodi, A., Tarot, S., Parrens, M., Al-Yaari, A., Pellarin, T., Rodríguez-Fernández, N., and Wigneron, J.-P.: The global SMOS Level 3 daily soil moisture and brightness temperature maps. Earth Syst. Sci. Data, 9(1), 293–315, doi: 10.5194/essd-9-293-2017, 2017.

Alshammari, L., Boyd, D., Sowter, A., Marshall, C., Anderson, R., Gilbert, P., Marsh, S., and Large, D.: Use of Surface Motion Characteristics Determined by InSAR to Assess Peatland Condition. J. Geophys. Res.-Biogeo., 125(1), 293–315, doi: 10.1029/2018JG004953, 2019.

Alvarez-Salazar, O., Hatch, S., Rocca, J., Rosen, P., Shaffer, S., Shen, Y., Sweetser, T., and Xaypraseuth, P.: Mission design for NISAR repeat-pass Interferometric SAR. Sensors, Systems, and Next-Generation Satellites XVIII, Amsterdam, Netherlands, 11 November 2014, 92410C, 2014.

Andresen, C., Lawrence, D., Wilson, C., McGuire, A. D., Koven, C., Schaefer, K., Jafarov, E., Peng, S., Chen, X., Gouttevin, I., Burke, E., Chadburn, S., Ji, D., Chen, G., Hayes, D., and Zhang, W.: Soil moisture and hydrology projections of the permafrost region – a model intercomparison. Cryosphere, 14(2), 445-459, doi: 10.5194/tc-14-445-2020, 2020.

Angert, A., Biraud, S., Bonfils, C., Henning, C., Buermann, W., Pinzon, J., Tucker, C., and Fung, I.: Drier summers cancel out the CO2 uptake enhancement induced by warmer springs. P. Natl. Acad. Sci. USA, 102(31), 10823-10827, doi: 10.1073/pnas.0501647102, 2005.

Armstrong, R., and Brodzik, M.: Recent northern hemisphere snow extent: A comparison of data derived from visible and microwave satellite sensors. Geophys. Res. Lett., 28(19), 3673–3676, doi: 10.1029/2000GL012556, 2001.

Attema, E., and Ulaby, F.: Vegetation modeled as a water cloud. Radio Sci., 13(2), 357-364, doi: 10.1029/RS013i002p00357, 1978.

Bachmann, M., Borla Tridon, D., De Zan, F., Krieger, G., and Zink, M.: Tandem-L observation concept - An acquisition scenario for the global scientific mapping machine. Proceedings of EUSAR 2016: 11th European Conference on Synthetic Aperture Radar, Hamburg, Germany, 6-9 June 2016, 1-5, 2016.

620 Baldocchi, D., Falge, E., Gu, L., Olson, R., Hollinger, D., Running, S., Anthoni, P., Bernhofer, C., Davis, K., Evans, R., Fuentes, J., Goldstein, A., Katul, G., Law, B., Lee, X., Malhi, Y., Meyers, T., Munger, W., Oechel, W., Paw U, K., Pilegaard, K., Schmid, H., Valentini, R., Verma, S., Vesala, T., Wilson, K., and Wofsy, S.: FLUXNET: A New Tool to Study the Temporal and Spatial Variability of Ecosystem–Scale Carbon Dioxide, Water Vapor, and Energy Flux Densities. B. Am. Meteorol. Soc., 82(11), 2415–2434, doi: 10.1175/1520-
625 0477(2001)082<2415:fantts>2.3.co;2, 2001.

Bamler, R.: Principles of Synthetic Aperture Radar. Surv. Geophys., 21, 147–157, doi: 10.1023/A:1006790026612, 2000.

Bartsch, A., Kidd, R., Pathe, C., Scipal, K., and Wagner, W.: Satellite radar imagery for monitoring inland wetlands in
630 boreal and sub-arctic environments. Aquat. Conserv., 17(3), 305-317, doi: 10.1002/aqc.836, 2007.

Bartsch, A., Widhalm, B., Kuhry, P., Hugelius, G., Palmtag, J., and Siewert, M. B.: Can C-band synthetic aperture radar be used to estimate soil organic carbon storage in tundra? Biogeosciences 13(19), 5453-5470; doi: 10.5194/bg-13-5453-2016, 2016.
635
Basist, A., Grody, N., Peterson, T., and Williams, C.: Using the special sensor microwave/imager to monitor land surface temperatures, wetness, and snow cover. J. Appl. Meteorol. Clim., 37(9), 888-911, doi: 10.1175/1520-0450(1998)037<0888:UTSSMI>2.0.CO;2, 1998.

640 Bindlish, R., Jackson, T., Cosh, M., Zhao, T., and O'Neill, P.: Global soil moisture from the Aquarius/SAC-D satellite: description and initial assessment. IEEE Geosci. Remote Sens,, 12(5), 923–927, doi: 10.1109/LGRS.2014.2364151, 2015.

Bircher, S., Demontoux, F., Razafindratsima, S., Zakharova, E., Drusch, M., Wigneron, J.-P., and Kerr, Y.: L-Band
645 Relative Permittivity of Organic Soil Surface Layers—A New Dataset of Resonant Cavity Measurements and Model Evaluation. Remote Sens., 8(12), 1024, doi:10.3390/rs8121024, 2016.

Björkman, M., Morgner, E., Cooper, E., Elberling, B., Klemedtsson, L., and Björk, R.: Winter carbon dioxide effluxes from Arctic ecosystems : An overview and comparison of methodologies. Gobal Biogeochem. Cy., 24,
650 GB3010, doi: 10.1029/2009GB003667, 2010.

Bokhorst, S., Pedersen, S., Brucker, L., Anisimov, O., Bjerke, J., Brown, R., Ehrich, D., Essery, R., Heilig, A., Ingvander, S., Johansson, C., Johansson, M., Jónsdóttir, I. S., Inga, N., Luojus, K., Macelloni, G., Mariash, H., McLennan, D., Rosqvist, G., Sato, A., Savela, H., Schneebeli, M., Sokolov, A., Sokratov, S., Terzago, S., Vikhamar-
655 Schuler, D., Williamson, S., Qiu, Y., and Callaghan, T.: Changing Arctic snow cover: A review of recent developments and assessment of future needs for observations, modeling, and impacts. Ambio, 45, 516-537, doi: 10.1007/s13280-016-0770-0, 2016.

Bowling, L., Kane, D., Gieck, R., Hinzman, L., and Lettenmaier, D.: The role of surface storage in a low-gradient Arctic
660 watershed. Water Resour. Res., 39(4), 1087, doi: 10.1029/2002WR001466, 2003.

Box, J., Colgan, W., Christensen, T. R., Schmidt, N. M., Lund, M., Parmentier, F.-J., Brown, R., Bhatt, U., Euskirchen, E. and Romanovsky, V.: Key indicators of Arctic climate change: 1971–2017. Environ. Res. Lett., 14(4), 045010, doi: 10.1088/1748-9326/aafc1b, 2019.

665

Bradshaw, C., and Warkentin, I.: Global estimates of boreal forest carbon stocks and flux. Global Planet. Change, 128, 24-30, doi: 10.1016/j.gloplacha.2015.02.004, 2015.

Brooks, P., Schmidt, S., and Williams, M.: Winter production of CO_2 and N_2O from alpine tundra: Environmental
670   controls and relationship to inter-system C and N fluxes. Oecologia, 110, 403-413, doi: 10.1007/PL00008814, 1997.

Brooks, P., and Williams, M.: Snowpack controls on nitrogen cycling and export in seasonally snow-covered catchments. Hydrol. Process., 13, 2177-2190, doi: 10.1002/(SICI)1099-1085(199910)13:14/15<2177::AID-
675   HYP850>3.0.CO;2-V, 1999.

Brown, J., Ferrians, O., Heginbottom, J., and Melnikov, E.: Circum-Arctic Map of Permafrost and Ground-Ice Conditions, Version 2. Boulder, Colorado USA. NSIDC: National Snow and Ice Data Center, doi: 10.7265/skbg-kf16, 2002.

680

Brucker, L., Dinnat, E., and Koenig, L.: Weekly gridded Aquarius L-band radiometer/scatterometer observations and salinity retrievals over the polar regions – Part 1: Product description. Cryosphere, 8(3), 905–913, doi: 10.5194/tc-8-905-2014, 2014.

685   Buchwitz, M., Schneising, O., Burrows, J., Bovensmann, H., and Reuter, M.: First direct observation of the atmospheric CO_2 year-to-year increase from space. Atmos Chem. Phys., 7(16), 4249-4256, doi: 10.5194/acp-7-4249-2007, 2007.

Callaghan, T., Johansson, M., Brown, R., Groisman, P., Labba, N., Radionov, V., Bradley, R., Blangy, S., Bulygina, O.,
690   Christensen, T., Colman, J., Essery, R., Forbes, B., Forchhammer, M., Golubev, V., Honrath, R., Juday, G., Meshcherskaya, A., Phoenix, G., Pomeroy, J., Rautio, A., Robinson, D., Schmidt, N., Serreze, M., Shevchenko, V., Shiklomanov, A., Shmakin, A., Sköld, P., Sturm, M., Woo, M., Woodm E. (2011). Multiple effects of changes in Arctic snow cover. Ambio, 40, 32-45, doi: 10.1007/s13280-011-0213-x

695   Carreiras, J., Quegan, S., Le Toan, T., Ho Tong Minh, D., Saatchi, S., Carvalhais, N., Reichstein, M., and Scipal, K.: Coverage of high biomass forests by the ESA BIOMASS mission under defense restrictions. Remote Sens. Environ., 196, 154-162, doi: 10.1016/j.rse.2017.05.003, 2017.

Chan, S., Bindlish, R., O'Neill, P., Njoku, E., Jackson, T., Colliander, A., Chen, F., Burgin, M., Dunbar, S., Piepmeier,
700   J., Yueh, S., Entekhabi, D., Cosh, M., Caldwell, T., Walker, J., Berg, A., Rowlandson, T., Pacheco, A., McNairn, H., Thibeault, M., Martinez- Fernández, J., González-Zamora, A., Bosch, D., Starks, P., Goodrich, D., Prueger, J., Palecki, M., Small, E., Zreda, M., Calvet, J., Crow, W., and Kerr., Y.: Assessment of the SMAP

passive soil moisture product. IEEE T. Geosci. Remote, 54, 4994–5007, doi: 10.1109/TGRS.2016.2561938, 2016.

705

Chan, S., Bindlish,, R., O'Neill, P., Jackson, T., Njoku, E., Dunbar, S., Chaubell, J., Piepmeier, J., Yueh, S., Entekhabi, D., Colliander, A., Chen, F., Cosh, M., Caldwell, T., Walker, J., Berg, A., McNairn, H., Thibeault, M., Martinez- Fernández, J., Uldall, F., Seyfried, M., Bosch, D., Starks, P., Collins, C., Prueger, J., Van der Velde, R., Asanuma, J., Palecki, M., Small, E., Zreda, M., Calvet, J., Crow, W., and Kerr, Y.: Development and assessment of the SMAP enhanced passive soil moisture product. Remote Sens. Environ., 204, 931–941, doi: 10.1016/j.rse.2017.08.025, 2018.

Chang, A., Foster, J., Hall, D., Rango, A., and Hartline, B.: Snow water equivalent estimation by microwave radiometry. Cold Reg. Sci. Technol., 5(3), 259–267, doi: 10.1016/j.jag.2011.10.014, 1982.

715

Chapin III, F., Woodwell, G., Randerson, J., Rastetter, E., Lovett, G., Baldocchi, D., Clark, D., Harmon, M., Schimel, D., Valentini, R., Wirth, C., Aber, J., Cole, J., Goulden, M., Harden, J., Heimann, M., Howarth, R., Matson, P., McGuire, A., Melillo, J., Mooney, H., Neff, J., Houghton, R., Pace, M., Ryan, M., Running, S., Sala, O., Schlesinger, W., and Schulze, E.-D.: Reconciling carbon-cycle concepts, terminology, and methods. Ecosystems, 9(7), 1041–1050, doi: 10.1007/s10021-005-0105-7, 2006.

Chen, X., Liu, L., and Bartsch, A.: Detecting soil freeze/thaw onsets in Alaska using SMAP and ASCAT data. Remote Sens. Environ., 220, 59–70, doi: 10.1016/j.rse.2018.10.010, 2019.

725 Chirici, G., Chiesi, M., Corona, P., Salvati, R., Papale, D., Fibbi, L., Sirca, C., Spano, D., Duce, P., Marras, S., Matteucci, G., Cescatti, A., and Maselli, F.: Estimating daily forest carbon fluxes using a combination of ground and remotely sensed data. Biogeosciences, 121(2), 266-279, doi: 10.1002/2015JG003019, 2016.

Chu, H., Baldocchi, D., John, R., Wolf, S., and Reichstein, M.: Fluxes all of the time? A primer on the temporal representativeness of FLUXNET. J. Geophys. Res.: Biogeosciences, 122(2), 289–307, doi: 10.1002/2016JG003576, 2017.

Ciais, P., Tan, J., Wang, X., Roedenbeck, C., Chevallier, F., Piao, S.-L., Moriarty, R., Broquet, G., Le Quéré, C., Canadell, J., Peng, S., Poulter, B., Liu, Z., and Tans, P.: Five decades of northern land carbon uptake revealed by the interhemispheric CO2 gradient. Nature, 568, 221-225, doi: 10.1038/s41586-019-1078-6, 2019.

Cohen, J., Rautiainen, K., Ikonen, J., Lemmetyinen, J., Smolander, T., Vehvilêinen, J., and Pulliainen, J.: A modeling-based approach for soil frost detection in the northern boreal forest region with C-Band SAR. IEEE T. Geosci. Remote, 57(2), 1069-1083, doi: 10.1109/TGRS.2018.2864635, 2019.

740

Colliander, A., Jackson, T., Bindlish, R., Chan, S., Das, N., Kim, S., Cosh, M., Dunbar, R., Dang, L., Pashaian, L., Asanuma, J., Aida, K., Berg, A., Rowlandson, T., Bosch, D., Caldwell, T., Caylor, K., Goodrich, D., al Jassar, H., Lopez-Baeza, E., Martínez Fernández, J., González-Zamora, A., Livingston, S., McNairn, H., Pacheco, A., Moghaddam, M., Montzka, C., Notarnicola, C., Niedrist, G., Pellarin, T., Prueger, J., Pulliainen, J., Rautiainen,

745   K., Ramos, J., Seyfried, M., Starks, P., Su, Z., Zeng, Y., van der Velde, R., Thibeault, M., Dorigo, W., Vreugdenhil, M., Walker, J. P., Wu, X., Monerris, A., O'Neill, P. E., Entekhabi, D., Njoku, E.G., Yueha, S.: Validation of SMAP surface soil moisture products with core validation sites. Remote Sens. Environ., 191, 215-231, doi: 10.1016/j.rse.2017.01.021, 2017.

750 Colliander, A., Reichle, R., Crow, W., Cosh, M., Chen, F., Chan, S., Das, N., Bindlish, R., Chaubell, J., Kim, S., Liu, Q., O'Neill, P., Dunbar, R. S., Dang, L., Kimball, J., Jackson, T., Al-Jassar, H., Asanuma, J., Bhattacharya, B., Berg, A., Bosch, D., Bourgeau-Chevez, L., Caldwell, T., Calvert, J.-C.,Collins, C. H., Jenson, K., Livingston, S., Lopez-Baeza, E., Martínez-Fernández, J., McNairn, H., Moghaddam, M., Montzka, C., Notarnicola, C., Pellarin, T., Greimeister-Pfeil, I., Pulliainen, J., Gpe, J., Hernández, R., Seyfried, M., Starks, P., Su, Z., van der
755   Velde, R., Zeng, Y., Thibeault, M., Vreugdenhil, M., Walker, J., Zribi, M., Entekhabi, D., and Yueh, S.: Validation of soil moisture data products from the NASA SMAP mission. IEEE J. Sel. Top. Appl., 15, 364-392, doi: 10.1109/JSTARS.2021.3124743, 2022.

Cui, Q., Shi, J., Du, J., Zhao, T., and Xiong, C.: An approach for monitoring global vegetation based on multiangular
760   observations from SMOS. IEEE J. Sel. Top. Appl. 8(2), 604–616, doi: 10.1109/JSTARS.2015.2388698, 2015.

Das, K., and Paul, P.: Present status of soil moisture estimation by microwave. Remote Sens., Cogent Geoscience, 1(1), 1084669, doi: 10.1080/23312041.2015.1084669, 2015.

765 Das, N., Entekhabi, D., Kim, S., Yueh, S. Dunbar, R. S., and Colliander, A.: SMAP/Sentinel-1 L2 Radiometer/Radar 30-Second Scene 3 km EASE-Grid Soil Moisture, Version 1. Boulder, Colorado USA. NASA National Snow and Ice Data Center Distributed Active Archive Center, doi: 10.5067/9UWR1WTHW1WN, 2017.

Das, B., Bordoloi, R., Deka, S., Paul, A., Pandey, P. K., Singha, L. B., Tripathi, O. P., Mishra, B. P., and Mishra, M.:
770   Above ground biomass carbon assessment using field, satellite data and model based integrated approach to predict the carbon sequestration potential of major land use sector of Arunachal Himalaya, India. Carbon Manag., 12(2), 201-214, doi: 10.1080/17583004.2021.1899753, 2021

Derksen, C., Xu, X., Scott Dunbar, R., Colliander, A., Kim, Y., Kimball, J. S., Black, T. A., Euskirchen, E., Langlois,
775   A., Loranty, M. M., Marsh, P., Rautiainen, K., Roy, A., Royer, A., and Stephens, J.: Retrieving landscape freeze/thaw state from Soil Moisture Active Passive (SMAP) radar and radiometer measurements. Remote Sens. Environ., 194, 48–62, doi: 10.1016/j.rse.2017.03.007, 2017.

Derksen, C., Burgess, D., Duguay, C., Howell, S., Mudryk, L., Smith, S., Thackeray, C., and Kirchmeier-Young, M.:
780   Changes in snow, ice, and permafrost across Canada. Canada's Changing Climate Report – Chapter 5, Government of Canada, Ottawa, Ontario, Canada, 194–260, 2019.

Dimitrov, D.D., Lafleur, P., Sonnentag, O., Talbot, J., Quinton, W.L.: Hydrology of peat estimated fron near-surface water contents. Hydrolog. Sci. J., 67(11), 1702-1721.

785

Dobson, M., Ulaby, F., Hallikainen, M., and El-Rayes, M.: Microwave dielectric behavior of wet soil - Part II: Dielectric mixing models. Geosci. Model Dev., GE-23, 35–46, doi: 10.1109/TGRS.1985.289498, 1985.

Dobson, M.., Ulaby, F., and Pierce, L.: Land-cover classification and estimation of terrain attributes using synthetic aperture radar. Remote Sens. Environ., 51(1), 199–214, doi: 10.1016/0034-4257(94)00075-X, 1995.

Dolant, C., Langlois, A., Brucker, L., Royer, A., Roy, A., and Montpetit, B.L Meteorological inventory of rain-on-snow events in the Canadian Arctic Archipelago and satellite detection assessment using passive microwave data. Phys. Geogr., 39(5), 428-444, doi: 10.1080/02723646.2017.1400339, 2018.

Dou, Y., Tian, F., Wigneron, J.P., Tagesson, T., Du, J., Brandt, M., Liu, Y., Zou, L., Kimball, J.S. and Fensholt, R.: Reliability of using vegetation optical depth for estimating decadal and interannual carbon dynamics. Remote Sens. Environ., 285, 113390, doi: 10.1016/j.rse.2022.113390, 2023.

Du, J., Kimball, J., Jones, L., Kim, Y., Glassy, J., and Watts, J.: A global satellite environmental data record derived from AMSR-E and AMSR2 microwave Earth observations. Earth Syst. Sci. Data, 9(2), 791–808, doi: 10.5194/essd-9-791-2017, 2017.

Du, J., Watts, J., Jiang, L., Lu, H., Cheng, X., Duguay, C., Farina, M., Qiu, Y., Kim, Y., Kimball, J., and Tarolli, P.: Remote sensing of environmental changes in cold regions: methods, achievements and challenges. Remote Sens., 11(16), 1952, doi: 10.3390/rs11161952, 2019.

Du, S., Liu, L., Liu, X., Guo, J., Hu, J., Wang, S., and Zhang, Y.: SIFSpec: Measuring solar-induced chlorophyll fluorescence observations for remote sensing of photosynthesis. Sensors, 19(13), 3009, doi: 10.3390/s19133009, 2019.

Du, J., Kimball, J.S., Bindlish, R., Walker, J.P. and Watts, J.D.: Local Scale (3-m) Soil Moisture Mapping Using SMAP and Planet SuperDove. Remote Sens., 14(15), 3812, doi: 10.3390/rs14153812, 2022.

Dubock, D., Spoto, F., Simpson, J., Spencer, D., Schutte, E., and Sontag, H.: The Envisat satellite and its integration. ESA Bulletin, 106, 26-45, 2001.

Duan, S.-B., Han, X.-J., Huang, C., Li, Z.-L., Wu, H., Qian, Y., Gao, M., Leng, P.: Land surface temperature retrieval from passive microwave satellite observations: state-of-the-art and future directions. Remote Sens., 12(16), 2573. doi: 10.3390/rs12162573

Edokossi, K., Calabia, A., Jin, S., and Molina, I.: GNSS-Reflectometry and Remote Sensing of Soil Moisture: A Review of Measurement Techniques, Methods, and Applications. Remote Sens., 12, 614, doi: 10.3390/rs12040614, 2020.

El-Amine, M., Roy, A., Koebsch, F., Baltzer, J., Barr, A., Black, A., Ikawa, H., Iwata, H., Kobayashi, H., Ueyama, M., and Sonnentag, O.: What explains the year-to-year variation in thestart and end of the photosynthetic growing

season of boreal black spruceforests? Agr. Forest Meteorol., 324, 109113, doi: 10.1016/j.agrformet.2022.109113, 2022.

830

Elbering, B.: Annual soil CO2 effluxes in the High Arctic: The role of snow thickness and vegetation type. Soil Biol. Biochem., 39, 646-654, doi: 10.1016/j.soilbio.2006.09.017, 2007.

El Hajj, M., Baghdadi, N., Zribi, M., and Bazzi, H.: Synergic Use of Sentinel-1 and Sentinel-2 Images for operational
835   soil moisture mapping at high spatial resolution over agricultural areas. Remote Sens., 9(12), 1292, doi: 10.3390/rs9121292, 2017.

El-Rayes, M., and Ulaby., F.: Microwave dielectric spectrum of vegetation-Part I: Experimental observations. IEEE T. Geosci. Remote, GE-25, 541-549, doi: 10.1109/TGRS.1987.289832, 1987.

840

Engman, E.: Applications of microwave remote sensing of soil moisture for water resources and agriculture. Remote Sens. Environ., 35(2-3), 213-226, doi: 10.1016/0034-4257(91)90013-V, 1991.

Entekhabi, D., Njoku, E., O'Neill, P., Kellogg, K., Crow, W., Edelstein, W., Entin, J., Goodman, S., Jackson, T., Jackson,
845   J., Kimball, J., Piepmeier, J., Koster, R., Martin, N., McDonald, K., Moghaddam, M., Moran, S., Reichle, R., Shi, J., Spencer, M., Thurman, S., Tsang, L., and Van Zyl, J.: The Soil Moisture Active Passive (SMAP) mission. P. IEEE, 98, 704–716, doi: 10.1109/JPROC.2010.2043918, 2010.

FAO - Food and Agriculture Organization of the United Nations: Global forest resources assessment 2000: main report.
850   FAO Forestry Paper 140, United Nations, Rome, Italy, 479 pages, 2001.

Fahnestock, J., Jones, M., Brooks, P., Walker, D., and Welker, J.: Winter and early spring CO_2 efflux from tundra communities of northern Alaska. J. Geophys. Res., 103, 29023–29027, doi: 10.1029/98JD00805, 1998.

855 Fahnestock, J., Jones, M., and Welker, J.: Wintertime CO_2 efflux from arctic soils: implications for annual carbon budgets. Gobal Biogeochem. Cy., 13, 775–779, doi: 10.1029/1999gb900006, 1999.

Fernández-Morán, R., Al-Yaari, A., Mialon, A., Mahmoodi, A., Al Bitar, A., De Lannoy, G., Rodríguez-Fernández, N., Lopez-Baeza, E., Kerr, Y., and Wigneron, J.-P.: SMOS-IC: An Alternative SMOS Soil Moisture and
860   Vegetation Visible Depth Product. Remote Sens., 9, 457, doi: 10.3390/rs9050457, 2017.

Fernández-Morán, R., Mialon, A., Al-Yaari, Mermoz, S., Bouvet, A., Richaume, P., Al Bitar, A., Al-Yaari, A., Brandt, M., Kaminski, T., Le Toan, T., Kerr, Y., and Wigneron, J.-P.: An evaluation of SMOS L-band vegetation visible depth (L-VOD) data sets: high sensitivity of L-VOD to above-ground biomass in Africa.
865   Biogeosciences, 15, 4627-4645, doi: 10.5194/bg-15-4627-2018, 2018.

Fiedler, S. and Sommer, M.: Methane emissions, groundwater levels and redox potentials of common wetland soils in a temperate-humid climate. Glob. Biogeochem. Cycles., 14(4), 1081-1093, doi: 10.1029/1999GB001255, 2000.

870   Figa-Saldaña, J., Wilson, J., Attema, E., Gelsthorpe, R., Drinkwater, M., and Stoffelen, A.: The advanced scatterometer (ASCAT) on the meteorological operational (MetOp) platform: A follow on for European wind scatterometers. Can. J. of Remote Sens., 28(3), 404–412, doi: 10.5589/m02-035, 2002.

Fily, M., Royer, A., Goïta, K., and Prigent, C.: A simple retrieval method for land surface temperature and fraction of
875   water surface determination from satellite microwave brightness temperatures in sub-arctic areas. Remote Sens. Environ., 85(3), 328-338, doi: 10.1016/S0034-4257(03)00011-7, 2003.

Fisher, J., Hayes, D., Schwalm, C., Huntzinger, D., Stofferahn, E., Schaefer, K., Luo, Y., Wullschleger, S., Goetz, S., Miller, C., Griffith, P., Chadburn, S., Chatterjee, A., Ciais, P., Douglas, T., Genet, H., Ito, A., Neigh, C., Poulter,
880   B., Rogers, B., Sonnentag, O., Tian, H., Wang, W., Xue, Y., Yang, Z.-L., Zeng, N., and Zhang, Z.: Missing pieces to modeling the Arctic-Boreal puzzle. Environ. Res. Lett., 13(2), 020202, doi: 10.1088/1748-9326/aa9d9a, 2018.

Forster, R., Long, D., Jezel, K., Brobot, S., and Anderson, M.: The onset of Arctic sea-ice snowmelt as detected with
885   passive- and active-microwave Remote Sens.. Ann. of Glaciol., 33, 85–93, doi:10.3189/172756401781818428, 2001.

Foster, A.C., Shuman, J.K., Rogers, B.M., Walker, X.J., Mack, M.C., Bourgeau-Chavez, L.L., Veraverbeke, S., Goetz, S.J.: Bottom-up drivers of future fire regimes in western boreal North America. Environ. Res. Lett., 17(2),
890   025006, doi : 10.1088/1748-9326/ac4c1e, 2022.

Frolking, S., Goulden, M.,Wofsy, S., Fan, S.-M., Sutton, D., Munger, J., Bazzaz, A., Daube, B., Crill, P., Aber, J., Band, L., Wang, X., Savage K., Moore, T., and Harriss, R.: Modeling temporal variability in the carbon balance of a spruce/moss boreal forest. Global Change Biol., 2, 343–366, doi: 10.1111/j.1365-2486.1996.tb00086.x, 1996.
895

Fu, Z., Stoy, P., Luo, Y., Chen, J., Sun, J., Montagnani, L., Wohlfahrt, G., Rahman, A., Rambal, S., Bernhofer, C., Wang, J., Shirkey, G., and Niu, S.: Climate controls over the net carbon uptake period and amplitude of net ecosystem production in temperate and boreal ecosystems. Agr. Forest Meteorol., 243, 9–18, doi: 10.1016/j.agrformet.2017.05.009, 2017.
900

Gasser, T., Crepin, L., Quilcaille, Y., Houghton, R., Ciais, P. and Obersteiner, M.: Historical CO2 emissions from land use and land cover change and their uncertainty. Biogeosciences, 17(15), 4075-4101, doi: 10.5194/bg-17-4075-2020, 2020.

905   Gauthier, S., Bernier, P., Kuuluvainen, T., Shvidenko, A., and Schepaschenko, D.: Boreal forest health and global change. Science, 349(6250), 819-822, doi: 10.1126/science.aaa9092, 2015.

Gloersen, P., and Barath, F.: A scanning multichannel microwave radiometer for Nimbus-G and SeaSat-A. IEEE J. Oceanic Eng., 2(2), 172–178, doi: 10.1109/JOE.1977.1145331, 1977.
910

Gough, C.: Terrestrial Primary Production: Fuel for Life. Nature Education Knowledge, 3(10), 28, 2011.

Grasso, M., Renga, A., Fasano, G., Graziano, M., Grassi, M., and Moccia, A.: Design of an end-to-end demonstration mission of a Formation-Flying Synthetic Aperture Radar (FF-SAR) based on microsatellites. Adv. Space Res., doi: 10.1016/j.asr.2020.05.051, 2021.

915

Grosse, G., Harden, J., Turetsky, M., McGuire, D., Camill, P., Tarnocai, C., Frolking, S., Schuur, E., Jorgenson, T., Marchenko, S., Romanovsky, V., Wickland, K., French, N., Waldrop, M., Bourgeau-Chavez, L., and Striegl, R.: Vulnerability of high-latitude soil organic carbonin North America to disturbance. J. Geophys. Res., 116,

920   G00K06, doi: 10.1029/2010JG001507, 2011.

Gruber, A., Scanlon, T., van des Schalie, R., Wagner, W., and Dorigo, E.: Evolution of the ESA CCI Soil Moisture climate data records and their underlying merging methodology. Earth Syst. Sci. Data, 11(2), 717-739, doi: 10.5194/essd-11-717-2019, 2019.

925

Ruiz-Pérez, G., and Vico, G.: Effects of Temperature and Water Availability on Northern European Boreal Forests. Front. For. Glob. Change, 3, 34, doi: 10.3389/ffgc.2020.00034, 2020.

Hallikainen, M., Ulaby, F., Dobson, M., El-rayes, M., and Wu, L.: Microwave Dielectric Behavior of Wet Soil-Part 1:

930   Empirical Models and Experimental Observations. IEEE T. Geosci. Remote, GE-23(1), 25-34, doi: 10.1109/TGRS.1985.289497, 1985.

Harrison, J., Sanders-DeMott, R., Reinmann, A., Sorensen, P., Phillips, N., and Templer, P.: Growing-season warming and winter soil freeze/thaw cycles increase transpiration in a northern hardwood forest. Ecology, 101(11),

935   e03173, doi: 10.1002/ecy.3173, 2020.

Hayes, J., McGuire, A., Kicklighter, D., Gurney, K., Burnside, T., and Melillo, J.: Is the northern high-latitude land-based CO_2 sink weakening?. Gobal Biogeochem. Cy.. 25(3), GB3018, doi: 10.1029/2010GB003813, 2011.

940 Hollinger, J., Peirce, J., and Poe, G.: SSM/I instrument evaluation. IEEE T. Geosci. Remote, 28(5), 781–790, doi: 10.1109/36.58964, 1990.

Holtzman, N., Anderegg, L., Kraatz, S., Mavrovic, A., Sonnentag, O., Pappas, C., Cosh, M., Langlois, A., Lakhankar, T., Tesser, D., Steiner, N., Colliander, A., Roy, A., and Konings, A.: L-band vegetation optical depth as an

945   indicator of plant water potential in a temperate deciduous forest stand. Biogeosciences, 18(2), 739-753, doi: 10.5194/bg-18-739-2021, 2021.

Hori, M., Sugiura, K., Kobayashi, K., Aoki, T, Tanikawa, T., Kuchiki, K., Niwano, M., and Enomoto, H.: A 38-year (1978–2015) Northern Hemisphere daily snow cover extent product derived using consistent objective criteria

950   from satellite-borne optical sensors. Remote Sens. Environ., 191, 402-418, doi: 10.1016/j.rse.2017.01.023, 2017.

Houghton, R.: Aboveground Forest Biomass and the Global Carbon Balance. Global Change Biol., 11(6), 945-958, doi: 10.1111/j.1365-2486.2005.00955.x, 2005.

955

Hu, F. S., Higuera, P., Duffy, P., Chipman, M., Rocha, A., Young, A., Kelly, R., and Dietze, M.: Arctic tundra fires: natural variability and responses to climate change. Front. Ecol. Environ., 13(7), 369-377, doi: 10.1890/150063, 2015.

960   Huang, H., Tsang, L., Njoku, E., Colliander, A., Liao, T.-H., and Ding, K.-H.: Propagation and Scattering by a Layer of Randomly Distributed Dielectric Cylinders Using Monte Carlo Simulations of 3D Maxwell Equations With Applications in Microwave Interactions With Vegetation. IEEE Access, 5, 11985-12003, doi: 10.1109/ACCESS.2017.2714620, 2017.

965   Huber, S., Villano, M., Younis, M., Krieger, G., Moreira, A., Grafmueller, B., and Wolters, R.: Tandem-L: Design Concepts for a Next-Generation Spaceborne SAR System. In Proceedings of the EUSAR 2016: 11th European Conference on Synthetic Aperture Radar, Hamburg, Germany, 6–9 June 2016, 1–5, 2016.

van Huissteden, J., and Dolman, A.: Soil carbon in the Arctic and the permafrost carbon feedback. Curr. Opin. Env. Sust.,
970   4(5), 545-551, doi: 10.1016/j.cosust.2012.09.008, 2012.

Huntzinger, D., Schaefer, K., Schwalm, C., Fisher, J., Hayes, D., Stofferahn, E., Carey, J., Michalak, A., Wei, Y., Jain, A., Kolus, H., Mao, J., Poulter, B., Shi, X., Tang, J., and Tian, H.: Evaluation of simulated soil carbon dynamics in Arctic-Boreal ecosystems. Environ. Res. Lett., 15(2), 025005, doi: 10.1088/1748-9326/ab6784, 2020.

975

IPCC (Intergovernmental Panel on Climate Change): Pörtner, H.-O. Roberts, D., Masson-Delmotte, V., Zhai, P., Tignor, M., Poloczanska, E., Mintenbeck, K., Alegría, A., Nicolai, M., Okem, A., Petzold, J., Rama, B., and Weyer, N.: Special Report on the Ocean and Cryosphere in a Changing Climate. In press., 750 pages, 2019.

980   Jarvis, P., and Linder, S.: Constraints to growth of boreal forests. Nature, 405, 904–905, doi: 10.1038/35016154, 2000.

Jackson T., and Schmugge T.: Vegetation effects on the microwave emission of soils. Remote Sens. Environ. 36(3), 203–212, doi: 10.1016/0034-4257(91)90057-D, 1991.

985   Jenson, J.: Remote sensingof the Environment: An Earth Resource Perspective, 2nd edition. Pearson Prentice Hall, Upper Saddle River, New Jersey, United States, 656 pages, 2006.

Jiménez-Muñoz, and G., Sobrino, J.: Error sources on the land surface temperature retrieved from thermal infrared single channel remote sensing data. Int. J. Remote Sens., 27(5), 999-1014, doi: 10.1080/01431160500075907, 2006.

990

Jones, L., Kimball, J., McDonald, K., Chan, S., Njoku, E., and Oechel, W.: Satellite microwave remote sensing of boreal and Arctic soil temperatures from AMSR-E. IEEE T. Geosci. Remote, 45(7), 2004–2018, doi: 10.1109/TGRS.2007.898436, 2007.

995   Jones, L.A., Ferguson, C.R., Kimball, J.S., Ke Zhang, Chan, S.T.K., McDonald, K.C., Njoku, E.G., Wood, E.F.: Satellite
         Microwave Remote Sensing of Daily Land Surface Air Temperature Minima and Maxima From AMSR-E.
         IEEE J. Sel. Top. Appl. Earth Obs. Remote Sens., 3(1), 111–123, doi:10.1109/jstars.2010.2041530, 2010.

       Jones, M., Jones, L., Kimball, J., and McDonald, K.: Satellite passive microwave remote sensing for monitoring global
1000   land surface phenology. Remote Sens. Environ., 115(4), 1102–1114, doi: 10.1016/j.rse.2010.12.015, 2011.

       Jones, L., Kimball, J., Reichle, R., Madani, N., Glassy, J., Ardizzone, J., Colliander, A., Cleverly, J., Desai, A., Eamus,
         D., Euskirchen, E., Hutley, L., Macfarlane, C., and Scott, R.: The SMAP Level 4 Carbon Product for
         Monitoring Ecosystem Land–Atmosphere CO_2 Exchange. IEEE T. Geosci. Remote, 55(11), 6517-6532, doi:
1005   10.1109/TGRS.2017.2729343, 2017.

       Kerr, Y., Waldteufel, P., Wigneron, J.-P., Delwart, S., Cabot, F., Boutin, J., Escorihuela, M., Font, J., Reul, N., Gruhier,
         C., and Juglea, S.: The SMOS mission: New tool for monitoring key elements of the global water cycle. IEEE
         T. Geosci. Remote, 98, 666–687, doi: 10.1109/JPROC.2010.2043032, 2010.
1010
       Kerr, Y., Waldteufel, P., Richaume, P., Wigneron, J., Ferrazzoli, P., Mahmoodi, A., Al Bitar, A., Cabot, F., Gruhier, C.,
         Juglea, S., Leroux, D., Mialon, A., and Delwart, S.: The SMOS soil moisture retrieval algorithm. IEEE T.
         Geosci. Remote., 50, 1384–1403, doi: 10.1109/TGRS.2012.2184548, 2012.

1015   Kilic, L., Prigent, C., Aires, F., Boutin, J., Heygster, G., Tonboe, R., Roquet, H., Jimenez, C., and Donlon, C.: Expected
         Performances of the Copernicus Imaging Microwave Radiometer (CIMR) for an All-Weather and High Spatial
         Resolution Estimation of Ocean and Sea Ice Parameters. J. Geophys. Res.-Oceans, 123(10), 7564-7580, doi:
         10.1029/2018JC014408, 2018.

1020   Kim, S.-B., van Zyl, J., Johnson, J., Moghaddam, M., Tsang, L., Colliander, A., Dunbar, R., Jackson, T., Jaruwatanadilok,
         S., West, R., Berg, A., Caldwell, T., Cosh, M., Goodrich, D., Livingston, S., López-Baeza, E., Rowlandson,
         T., Thibeault, M., Walker, J., Entekhabi, D., Njoku, E., O'Neill, P., Yueh, S.: Surface Soil Moisture Retrieval
         Using the L-Band Synthetic Aperture Radar Onboard the Soil Moisture Active–Passive Satellite and Evaluation
         at Core Validation Sites. IEEE T. Geosci. Remote, 55(4), 1897-1914, doi: 10.1109/TGRS.2016.2631126, 2017.
1025
       Kim, Y., Kimball, J., Zhang, K., and McDonald, K.: Satellite detection of increasing Northern Hemisphere non-frozen
         seasons from 1979 to 2008: Implications for regional vegetation growth. Remote Sens. Environ., 121, 472-487,
         doi: 10.1016/j.rse.2012.02.014, 2012.

1030   Kim, Y., Kimball, J., Xu, X., Dunbar, S., Colliander, A., and Derksen, C.: Global Assessment of the SMAP Freeze/Thaw
         Data Record and Regional Applications for Detecting Spring Onset and Frost Events. Remote Sens., 11(11),
         1317, doi: 10.3390/rs11111317, 2019.

Kimball, J., McDonald, K., Keyser, A. R., Frolking, S., and Running, S.: Application of the NASA Scatterometer (NSCAT) for determining the Daily Frozen and Nonfrozen Landscape of Alaska. Remote Sens. Environ, 75(1), 113-126, doi: 10.1016/S0034-4257(00)00160-7, 2001.

Kimball, J., Zhao, M., McDonald, K., Heinsch, F. A., and Running, S.: Satellite observations of annual variability in terrestrial carbon cycles and seasonal growing seasons at high northern latitudes. Proc. Spie, Microwave Remote Sensing of the Atmosphere and Environment IV, 5654, doi: 10.1117/12.578815, 2004a.

Kimball, J., McDonald, K., Running, S., and Frolking, S.: Satellite radar Remote sensingof seasonal growing seasons for boreal and subalpine evergreen forests. Remote Sens. Environ., 90, 243-258, doi: 10.1016/j.rse.2004.01.002, 2004b.

Kimball, J., Jones, L., Zhang, K., Heinsch, F. A., McDonald, K., and Oechel, W.: A Satellite Approach to Estimate Land-Atmosphere CO2 Exchange for Boreal and Arctic Biomes Using MODIS and AMSR-E. IEEE T. Geosci. Remote, 47(2), 569-587, doi: 10.1109/TGRS.2008.2003248, 2009.

Kimball, J., Jones, L., Glassy, J., Stavros, N., Madani, N., Reichle, R., Jackson, T., and Colliander, A.: Soil Moisture Active Passive Mission L4_C Data Product Assessment (Version 2 Validated Release). MAO Office Note No. 13(Version 1.0), NASA Goddard Space Flight Center, Greenbelt, Maryland, United States, 37 pages, 2017.

Köcher, P., Horna, V., and Leuschner, C.: Stem water storage in five coexisting temperate broad-leaved tree species: significance, temporal dynamics and dependence on tree functional traits. Tree Physiology, 33(8), 817–832, doi: 10.1093/treephys/tpt055, 2013.

Kohn, J., and Royer, A.: AMSR-E data inversion for soil temperature estimation under snow cover. Remote Sens. Environ., 114, 2951-2961.

Konings, A., Piles, M., Das N., and Entekhabi, D.: L-band vegetation visible depth and effective scattering albedo estimation from SMAP. Remote Sens. Environ., 198, 460-470, doi: 10.1016/j.rse.2017.06.037, 2017.

Konings, A., Rao, K., and Steele-Dunne, S.: Macro to micro: microwave Remote sensing of plant water content for physiology and ecology. New Phytol., 223(3), 1166-1172, doi: 10.1111/nph.15808, 2019.

Konings, A., Holtzman, N., Rao, K., Xu, L., and Saatchi, S.: Interannual Variations of Vegetation Optical Depth are Due to Both Water Stress and Biomass Changes. Geophys. Res. Lett., 48(16), e2021GL095267, doi: 10.1029/2021GL095267, 2021.

Kerr, Y., Waldteufel, P., Richaume, P., Wigneron, J., Ferrazzoli, P., Mahmoodi, A., Al Bitar, A., Cabot, F., Gruhier, C., Juglea, S., Leroux, D., Mialon, A., and Delwart, S.: The SMOS soil moisture retrieval algorithm. IEEE T. Geosci. Remote, 50(5), 1384-1403, doi: 10.1109/TGRS.2012.2184548, 2012.

1075 Krieger, G., Moreira, A., Zink, M., Hajnsek, I., Huber, S., Villano, M., Papathanassiou, K., Younis, M., Lopez Dekker, P., Pardini, M., Schulze, D., Bachmann, M., Borla Tridon, D., Reimann, J., Bräutigam, B., Steinbrecher, U., Tiendra, C., Sanjuan Ferrer, M., Zonno, M., Eineder, M., De Zan, F., Parizzi, A., Fritz, T., Diedrich, E., Maurer, E., Münzenmayer, R., Grafmüller, B., Wolters, R., te Hennepe, F., Ernst, R., and Bewick, C.: Tandem-L: Main results of the phase a feasibility study," 2016 IEEE International Geoscience and Remote Sensing Symposium
1080 (IGARSS), Beijing, China, 10-15 July 2016, 2116-2119, doi: 10.1109/IGARSS.2016.7729546, 2016.

Krishan, P., Meyers, T., Hook, S., Heuer, M., Senn, D., and Dumas, E.: Intercomparison of In Situ Sensors for Ground-Based Land Surface Temperature Measurements. Sensors, 20(18), 5268, doi: 10.3390/s20185268, 2020.

1085 Lai, D.: Methane Dynamics in Northern Peatlands: A Review. Pedosphere, 19(4), 409-421, doi: 10.1016/S1002-0160(09)00003-4, 2009.

Lakhankar, T., Krakauer, N., and Khanbilvardi, R.: Applications of microwave Remote sensing of soil moisture for agricultural applications. Int. j. terraspace sci. eng., 2(1), 81-91, doi: 10.1.1.701.7873, 2009.
1090
Larue, F., Royer, A., De Sève, D., Langlois, A., Roy, A., and Brucker, L.: Validation of GlobSnow-2 snow water equivalent over Eastern Canada, Remote Sens. Environ., 194, 264-277, doi: 10.1016/j.rse.2017.03.027, 2017.

Larue, F., Royer, A., De Sève, D., Roy, A., and Cosme, E.: Assimilation of passive microwave AMSR-2 satellite
1095 observations in a snowpack evolution model over northeastern Canada, Hydrol. Earth Syst. Sci., 22, 5711–5734, doi:10.5194/hess-22-5711-2018, 2018.

Lawrence, H., Wigneron, J.-P., Richaume, P., Novello, N., Grant, J., Mialon, A., Al Bitar, A., Merlin, O., Guyon, D., Leroux, D., Bircher, S., and Kerr, Y.: Comparison between SMOS Vegetation Visible Depth products and
1100 MODIS vegetation indices over crop zones of the USA. Remote Sens. Environ., 140, 396–406, doi: 10.1016/j.rse.2013.07.021, 2014.

Leanza, A., Manzoni, M., Monti-Guarnieri, A., and di Clemente, M.: LEO to GEO-SAR Interferences: Modelling and performance evaluation. Remote Sens., 11(14), 1720, doi: 10.3390/rs11141720, 2019.
1105
Lee, J.-S., Grunes, M., and Pottier, E.: Quantitative comparison of classification capability: fully polarimetric versus dual and single-polarization SAR. IEEE T. Geosci. Remote, 39(11), 2343-2351, doi: 10.1109/36.964970, 2001.

Lees, K., Quaife, T., Artz, R., Khomik, M., and Clarl, J.: Potential for using remote sensing to estimate carbon fluxes
1110 across northern peatlands – A review. Sci. Total Environ., 615, 857-874, doi: 10.1016/j.scitotenv.2017.09.103, 2018.

Le Toan, T., Quegan, S., Davidson, M., Balzter, H., Paillou, P., Papathanassiou, K., Plummer, S., Rocca, F., Saatchi, S., Shugart, H., and Ilander, L.: The BIOMASS mission: Mapping global forest biomass to better understand the
1115 terrestrial carbon cycle. Remote Sens. Environ., 115, 2850-2860, doi: 10.1016/j.rse.2011.03.020, 2011.

Li, Q., Kelly, R., Leppanen, L., Vehvilainen, J., Kontu, A., Lemmetyinen, J., and Pulliainen, J.: The influence of thermal properties and canopy-intercepted snow on passive microwave transmissivity of a scots pine. IEEE T. Geosci. Remote, 57(8), 5424-5433, doi: 10.1109/TGRS.2019.2899345, 2019.

1120

Li, W., Cardellach, E., Ribó, S., Oliveras, S., and Rius, A.: Exploration of Multi-Mission Spaceborne GNSS-R Raw IF Data Sets: Processing, Data Products and Potential Applications. Remote Sens., 14, 1344. doi: 10.3390/rs14061344, 2022.

1125   Li, X., Wigneron, J.P., Fan, L., Frappart, F., Simon H., Colliander, A., Ebtehaj A., Gao L., Fernandez-Moran R., Liu X.Z., Wang M.j., Ma H.l., Moisy C., and Ciais P.: A new SMAP soil moisture and vegetation optical depth product (SMAP-IB): Algorithm, assessment and inter-comparison. Remote Sens. Environ. 271, 112921, doi: 10.1016/j.rse.2022.112921, 2022.

1130   Lieffers, V., and Rothwell, R.: Rooting of peatland black spruce and tamarack in relation to depth of water table. Can. J. Bot., 65, 817-821, doi: 10.1139/b87-111, 1987.

Lievens, H., Demuzere, M., Marshall, H.-P., Reichle, R., Brucker, L., Brangers, I., de Rosnay, P., Dumont, M., Girotto, M., Immerzeel, W., Jonas, T., Kim, E., Koch, I., Marty, C., Saloranta, T., Schöber, J., and De Lannoy, G.:
1135   Snow depth variability in the Northern Hemisphere mountains observed from space. Nat. Commun., 10(1), 4629, doi: 10.1038/s41467-019-12566-y, 2019.

Liljedahl, A., Boike, J., Daanen, R., Fedorov, A., Frost, G., Grosse, G., Hinzman, L., Iijma, Y., Jorgenson, J., Matveyeva, N., Necsoiu, M., Raynolds, M., Romanovsky, V., Schulla, J., Tape, K., Walker, D., Wilson, C., Yabuki, H.,
1140   and Zona, D.: Pan-Arctic ice-wedge degradation in warming permafrost and its influence on tundra hydrology. Nat. Geosci., 9(4), 312–318, doi: 10.1038/ngeo2674, 2016.

Liu, X. Wigneron J.-P., Fan, L., Frappart, F., Ciais, P., Baghdadi, N., Zribi, M., Jaghuber, T., Li, X., Wang, M., Bai, X., and Moisy, C.: ASCAT IB: A radar-based vegetation optical depth retrieved from the ASCAT scatterometer
1145   satellite, Remote Sens. Environ., 264, 112587, doi: 10.1016/j.rse.2021.112587, 2021.

Liu Y., van Dijk, A., de Jeu, R., Canadell, J., McCabe, M., Evans, J., and Wang, G.: Recent reversal in loss of global terrestrial biomass. Nat. Clim. Change, 5, 470–474, doi: 10.1038/nclimate2581, 2011a.

1150   Liu Y., A., de Jeu, R., J., McCabe, M., Evans, J., and van Dijk, A.: Global long-term passive microwave satellite-based retrievals of vegetation visible depth. Geophys. Res. Lett., 38(18), L18402, doi: 10.1029/2011GL048684, 2011b.

Liu, Y. Holtzman, N., and Konings, A.: Global ecosystem-scale plant hydraulic traits retrieved using model-data fusion.
1155   Hydrol. Earth Syst. Sc., 25, 2399-2417, doi: 10.5194/hess-25-2399-2021, 2021.

Liu, Z., Kimball, J., Parazoo, N., Ballantyne, A., Wang, W., Madani, N., Pan, C., Watts, J., Reichle, R., Sonnentag, O., Marsh, P., Hurkuk, M., Helbig, M., Quinton, W., Zona, D., Ueyama, M., Kobayashi, H., and Euskirchen, E.:

Increased high-latitude photosynthetic carbon gain offset by respiration carbon loss during an anomalous warm
1160   winter to spring transition. Global Change Biol., 26(2), 682-696, doi: 10.1111/gcb.14863, 2020.

Loisel, J., Gallego-Sala, A.V., Amesbury, M.J., Magnan, G., Anshari, G., Beilman, D.W., Benavides, J.C., Blewett, J.,
        Camill, P., Charman, D.J., Chawchai, S., Hedgpeth, A., Kleinen, T., Korhola, A., Large, D., Mansilla, C.A.,
        Müller, J., van Bellen, S., West, J.B., Yu, Z., Bubier, J.L., Garneau, M., Moore, T., Sannel, A.B.K., Page, S.,
1165   Väliranta, M., Bechtold, M., Brovkin, V., Cole, L.E.S., Chanton, J.P., Christensen, T.R., Davies, M.A., De
        Vleeschouwer, F., Finkelstein, S.A., Frolking, S., Galka, M., Gandois, L., Girkin, N., Harris, L.I., Heinemeyer,
        A., Hoyt, A.M., Jones, M.C., Joos, F., Juutinen, S., Kaiser, K., Lacourse, T., Lamentowicz, M., Larmola, T.,
        Leifeld, J., Lohila, A., Milner, A.M., Minkkinen, K., Moss, P., Naafs, B.D.A., Nichols, J., O'Donnel, J., Payne,
        R., Philben, M., Piilo, S., Quillet, A., Ratnayake, A.S., Roland, T.P., Sjögersten, S., Sonnentag, O., Swindles,
1170   G.T., Swinnen, W., Talbot, J., Treat, C., Valach, A.C., Wu, J. : Expert assessment of future vulnerability of the
        global peatland carbon sink. Nat. Clim. Change, 11, 70-77, 2021.

Lönnqvist, A., Rauste, Y., Molinier, M., and Häme, T.: Polarimetric SAR Data in Land Cover Mapping in Boreal Zone.
        IEEE T. Geosci. Remote, 48(10), 3652-3662, doi: 10.1109/TGRS.2010.2048115, 2010.
1175
Lorente, A., Borsdorff, T., Butz, A., Hasekamp, O., ass de Brugh, J., Schneider, A., Wu, L., Hase, F., Kive, R., Wunch,
        D., Pollard, D., Shiomi, K., Deutscher, N., Velazco, V., Roehl, C., Wennberg, P., Warneke, T., and Landgraf,
        J.: Methane retrieved from TROPOMI: improvement of the data product and validation of the first 2 years of
        measurements. Atmos. Meas. Tech., 14, 665,684, doi: 10.5194/amt-14-665-2021, 2021.
1180
Luojus, K., Pulliainen, J., Takala, M., Lemmetyinen, J., Mortimer, C., Derksen, C., Mudryk, L., Moisander, M., Hiltunen,
        M., Smolander, T., Ikonen, J., Cohen, J., Salminen, M., Norberg, J., Veijola, K., and Venäläinen, P.: GlobSnow
        v3.0 Northern Hemisphere snow water equivalent dataset. Sci. Data, 8, 163, doi: 10.1038/s41597-021-00939-
        2, 2021.
1185
Maeda, T., Taniguchi, Y., and Imaoka, K.: GCOM-W1 AMSR2 Level 1R Product: Dataset of brightness temperature
        modified using the antenna pattern matching technique. IEEE T. Geosci. Remote, 54(2), 770-782, doi:
        10.1109/TGRS.2015.2465170, 2016.

1190   Magney, T., Bowling, D., Logan, B., Grossmann, K., Stutz, J., Blanken, P., Burns, S., Cheng, R., Garcia, M., Köhler, P.,
        Lopez, S., Parazoo, N., Raczka, B., Schimel, D., and Frankenberg, C.: Mechanistic evidence for tracking the
        seasonality of photosynthesis with solar-induced fluorescence. P. Natl. A. Sci. USA, 116(24), 11640-11645,
        doi: 10.1073/pnas.1900278116, 2019.

1195   Mao, J., Ribes, A., Yan, B., Shi, X., Thornton, P., Séférian, R., Ciais, P., Myneni, R., Douville, H., Piao, S., Zhu, Z.,
        Dickinson, R., Dai, Y., Ricciuto, D., Jin, M., Hoffman, F., Wang, B., Huang, M., and Lian, X.: Human-induced
        greening of the northern extratropical land surface. Nat. Clim. Change, 6, 959–963, doi: 10.1038/nclimate3056,
        2016.

1200   Mao, K., Zuo, Z., Shen, X., Xu, T., Gao, C., and Liu, G.: Retrieval of land-surface temperature from AMSR2 data using a deep dynamic learning neural network. Chinese Geogr. Sci., 28(1), 1-11, doi: 10.1007/s11769-018-0930-1, 2018.

Marchand, N., Royer, A., Krinner, G., Roy, A., Langlois, A., and Vargel, C.: Snow-covered soil temperature retrieval in
1205   Canadian Arctic permafrost areas, using a land surface scheme informed with satellite remote sensing data. Remote Sens., 10, 1703.

Marghany, M.: Principle theories of synthetic aperture radar. Synthetic aperture radar imaging mechanism for oil spills. Gulf Professional Publishing, United States, 322 pages (127–150), 2019.
1210

Matheny, A., Bohrer., G., Garrity, S., Morin, T., Howard, C., and Vogel, C.: Observations of stem water storage in trees of opposing hydraulic strategies. Ecosphere, 6(9), 1-13, doi: 10.1890/ES15-00170.1, 2015

Matheny, A., Mirfenderesgi, G., and Bohrer., G.: Trait-based representation of hydrological functional properties of
1215   plants in weather and ecosystem models. Plant Diversity, 39(1), 1-12, doi: 10.1016/j.pld.2016.10.001, 2017a.

Matheny, A., Garrity, S., and Bohrer., G.: The calibration and use of capacitance sensors to monitor stem water content in trees. Jove-J. Vis. Exp., 130, 57062, doi: 10.3791/57062, 2017b.

1220   Matthews, E., Johnson, M.S., Genovese, V., Du, J., and Bastviken, D.: Methane emission from high latitude lakes: methane-centric lake classification and satellite-driven annual cycle of emissions. Sci. Rep., 10, 12465, doi: 10.1038/s41598-020-68246-1, 2020.

McMahon, S., Parker, G., and Miller, D.: Evidence for a recent increase in forest growth. P. Natl. A. Sci. USA, 107(8),
1225   3611-3615, doi: 10.1073/pnas.0912376107, 2010.

Meloche, J., Langlois, A., Rutter, N., Royer, A., King, J., Walker, B., Marsh, P., and Wilcox, E.: Characterizing tundra snow sub-pixel variability to improve brightness temperature estimation in satellite SWE retrievals. Cryosphere, 16, 87–101 doi: 10.5194/tc-16-87-2022, 2022.
1230

Melton, J., Arora, V., Wisernig-Cojoc, E., Seiler, C., Fortier, M., Chan, E., and Teckentrup, L.: CLASSIC v1.0: the open-source community successor to the Canadian Land Surface Scheme (CLASS) and the Canadian Terrestrial Ecosystem Model (CTEM) – Part 1: Model framework and site-level performance. Geosci. Model Dev., 13, 2825–2850, doi: 10.5194/gmd-13-2825-2020, 2020.
1235

Merchant, M., Adams, J., Berg, A., Baltzer, J., Quinton, W., and Chasmer, L.: Contributions of C-Band SAR data and polarimetric decompositions to subarctic boreal peatland mapping. IEEE J. Sel. Top. Appl., 10(4), 1467-1482, doi: 10.1109/JSTARS.2016.2621043, 2017.

1240   Merchant, M., Warren, R., Edwards, R., and Kenyon, J.: An object-based assessment of multi-wavelength SAR, optical imagery and topographical datasets for operational wetland mapping in boreal Yukon, Canada. Can. J. Remote Sens., 45(3-4), 308-332, doi: 10.1080/07038992.2019.1605500, 2019.

        Merchant, M., Obadia, M., Brisco, B., DeVries, B., and Berg, A.: Applying machine learning and time-series analysis on
1245   Sentinel-1A SAR/InSAR for characterizing arctic tundra hydro-ecological condition. Remote Sens., 14(5), doi: 10.3390/rs14051123.

        Merzouki, A., McNairn, H., and Pacheco, A.: Mapping soil moisture using RADARSAT-2 data and local autocorrelation statistics. IEEE J. Sel. Top. Appl., 4(1), 128–137, doi: 10.1109/JSTARS.2011.2116769, 2011.

1250

        Mialon, A., Royer, A., Fily, M., and Picard, G.: Daily microwave-derived surface temperature over Canada/Alaska. J. Appl. Meteorol. Clim., 46(5), 591-604, doi: 10.1175/JAM2485.1, 2007.

        Mialon, A., Rodríguez-Fernández, N., Santoro, M., Saatchi, S., Mermoz, S., Bousquet, E., and Kerr, Y.: Evaluation of
1255   the sensitivity of SMOS L-VOD to forest above-ground biomass at global scale. Remote Sens., 12(9), 1450, doi: 10.3390/rs12091450, 2020.

        Mikan, C., Schimel, J., and Doyle, A.: Temperature controls of microbial respiration above and below freezing in Arctic tundra soils. Soil Biol. Biochem., 34, 1785–1795, doi: 10.3390/rs12091450, 2002.

1260

        Miner, K.R., Turesky, M.R., Malina, E., Bartsch, A., Tamminen, J., McGuire, A.D., Fix, A., Sweeney, C., Elder, C.D., and Miller, C.E.: Permafrost carbon emissions in a changing Arctic. Nat. Rev. Earth Environ., 3, 55-67.

        Mironov, V., De Roo, R., and Savin, I.: Temperature-Dependable Microwave Dielectric Model for an Arctic Soil. IEEE
1265   T. Geosci. Remote, 48(6), 585–589, doi: 10.1109/TGRS.2010.2040034, 2010.

        Mironov, V., and Savin, I.: A temperature-dependent multi-relaxation spectroscopic dielectric model for thawed and frozen organic soil at 0.05–15 GHz. Phys. Chem. Earth Parts ABC, 83–84, 57–64, doi: 10.1016/j.pce.2015.02.011, 2015.

1270
        Misra, T., Jha, A., Putrevu, D., Rao, J., Dave, D., and Rana, S.: Ground calibration of multifrequency ScanningMicrowave radiometer (MSMR). IEEE T. Geosci. Remote, 40(2), 504-508, doi: 10.1109/36.992823, 2002.

        Mo, T., Choudhury, B., Schmugge, T., Wang, J., and Jackson, T.: A model for microwave emission from vegetation-
1275   covered fields. J. Geophys. Res., 87, 11229–11237, doi: 10.1029/JC087iC13p11229, 1982.

        Moreira, A., Bachmann, M., Balzer, W., Tridon, D., Diedrich, E., Fritz, T., Grigorov, C., Kahle, R., Krieger, G., Hajnsek, I., Huber, S., Jörg, H., Klenk, P., Lachaise, M., Maier, M., Maurer, E., Papathanassiou, K., Parizzi, A., Prats, P., Reimann, J., Rodriguez, M., Schättler, B., Schwinger, M., Schulze, D., Steinbrecher, U., Villano, M.,
1280   Younis, M., De Zan, F., Zink, M., and Zonno, M.: Tandem-L: Project Status and Main Findings of the Phase

Bl Study. IGARSS 2018 - 2018 IEEE International Geoscience and Remote sensing Symposium, Valencia, Spain, 22-27 July 2018, 8667-8670, doi: 10.1109/IGARSS.2018.8518591, 2018.

Morrissey, L., Durden, S., Livingston, G., Steam, J., and Guild, L.: Differentiating methane source areas in Arctic environments with multitemporal ERS-1 SAR data. IEEE T. Geosci. Remote, 34(3), 667–673, doi: 10.1109/36.499746, 1996.

Mortimer, C., Mudryk, L., Derksen, C., Luojus, K., Brown, R., Kelly, R., and Tedesco, M.: Evaluation of long-term Northern Hemisphere snow water equivalent products. Cryosphere, 14, 1579-1594, doi: 10.5194/tc-14-1579-2020, 2020.

Mortin, J., Schrøder, T., Walløe Hansen, A., Holt, B., and McDonald, K.: Mapping of seasonal freeze-thaw transitions across the pan-Arctic land and sea ice domains with satellite radar. J. Geophys. Res.-Oceans, 117(C8), doi: 10.1029/2012JC008001, 2012.

Mu, Q., Zhao, M., Heinsch, F. A., Liu, M., Tian, H., and Running, S.: Evaluating water stress controls on primary production in biogeochemical and remote sensing based models. Biogeosciences, 112(G1), doi: 10.1029/2006JG000179, 2007.

Murfitt, J., and Duguay, C.: 50 years of lake ice research from active microwave remote sensing: Progress and prospects. Remote Sens. Environ., 264, 112616, doi: 10.1016/j.rse.2021.112616, 2021.

Myers-Smith, I. H., Forbes, B., Wilmking, M., Hallinger, M., Lantz, T., Blok, D., Tape, K., Macias-Fauria, M., Sass-Klaassen, U., Lévesque, E., Boudreau, S., Ropars, P., Hermanutz, L., Trant, A., Collier, L., Weijers, S., Rozema, J., Rayback, S., Schmidt, N., Schaepman-Strub, G., Wipf, S., Rixen, C., Ménard, C., Venn, S., Goetz, S., Andreu-Hayles, L., Elmondorf, S., Ravolainen, V., Welker, J., Grogan, P., Epstein, H., and Hik, D.: Shrub expansion in tundra ecosystems: dynamics, impacts and research priorities. Environ. Res. Lett., 6(4), 045509, doi: 10.1088/1748-9326/6/4/045509, 2011.

Myers-Smith, I. H., Kerby, J., Phoenix, G., Bjerke, J., Epstein, H., Assmann, J., John, C., Andreu-Hayles, L., Angers-Blondin, S., Beck, P., Berner, L., Bhatt, U., Bjorkman, A., Blok, C., Bryn, A., Christiansen, C., Cornelissen, J. H. C., Cunliffe, A., Elmendorf, S., Forbes, B., Goetz, S., Hollister, R., de Jong, R., Loranty, M., Macias-Fauria, M., Maseyk, K., Normand, S., Olofsson, J., Parker, T., Parmentier, F.-J., Post. E., Schaepman-Strub, G., Stordal, F., Sullivan, P., Thomas, H., Tømmervik, H., Treharne, R., Tweedie, C., Walker, D., Wilmking, M., and Wipf, S.: Complexity revealed in the greening of the Arctic. Nat. Clim. Change, 10, 106-117, doi: 10.1038/s41558-019-0688-1, 2020.

Naeimi, V., Scipal, K., Bartalis, Z., Hasenauer, S., and Wagner, W.: An Improved Soil Moisture Retrieval Algorithm for ERS and METOP Scatterometer Observations. IEEE T. Geosci. Remote, 47(7), 1999–2013, doi: 10.1109/TGRS.2008.2011617, 2009.

Naeimi, V., Paulik, C., Bartsch, A., Wagner, W., Kidd, R., Park, S.-E. Elger, K., and Boike, J.: ASCAT Surface State Flag (SSF): Extracting Information on Surface Freeze/Thaw Conditions From Backscatter Data Using an Empirical Threshold-Analysis Algorithm. IEEE T. Geosci. Remote, 50(7), 2566-2582, doi: 10.1109/TGRS.2011.2177667, 2012.

Nagler, T., and Rott, H.: Retrieval of wet snow by means of multitemporal SAR data. IEEE T. Geosci. Remote, 38(2), 754-765, doi: 10.1109/36.842004, 2000.

Natali, S.,Watts, J., Rogers, B., Potter, S., Ludwig, S., Selbmann, A.-K., Sullivan, P., Abbott, B., Arndt, K., Birch, L., Björkman, M., Bloom, A., Celis, G., Christensen, T., Christiansen, C., Commane, R., Cooper, E., Crill, P., Czimczik, C., Davydov, S., Du, J., Egan, J., Elberling, B., Euskirchen, E., Friborg, T., Genet, H., Göckede, M., Goodrich, J., Grogan, P., Helbig, M., Jafarov, E., Jastrow, J., Kalhori, A., Kim, Y., Kimball, J., Kutzbach, L., Lara, M., Larsen, K., Lee, B.-Y., Liu, Z., Loranty, M., Lund, M., Lupascu, M., Madani, N., Malhotra, A., Matamala, R., McFarland, J., McGuire, A., Michelsen, A., Minions, C., Oechel, W., Olefeldt, D., Parmentier, F.-J., Pirk, N., Poulter, B., Quinton, W., Rezanezhad, F., Risk, D., Sachs, T., Schaefer, K., Schmidt, N., Schuur, E., Semenchuk, P., Shaver, G., Sonnentag, O., Starr, G., Treat, C., Waldrop, M., Wang, Y., Welker, J., Wille, C., Xu, X., Zhang, Z., Zhuang, Q., and Zona, D.: Large loss of CO_2 in winter observed across the northern permafrost region. Nat. Clim. Change, 9, 852-857, doi: 10.1038/s41558-019-0592-8, 2019.

Neumann, M., Saatchi, S., Ulander, L., and Fransson, J.: Assessing performance of L- and P-Band polarimetric interferometric SAR data in estimating boreal forest above-ground biomass. IEEE T. Geosci. Remote, 50(3), 714–726, doi: 10.1109/TGRS.2011.2176133, 2012.

Osińska-Skotak, K.: Studies of soil temperature on the basis of satellite data. International Agrophysics, 21(3), 275–284, 2007.

Pallandt, M., Kumar, J., Mauritz, M., Schuur, E., Virkkala, A.-M., Celis, G., Hoffman, F. and Göckede, M.: Representativeness assessment of the pan-Arctic eddy covariance site network and optimized future enhancements. Biogeosciences, 19(3), 559-583, doi: 10.5194/bg-19-559-2022, 2022.

Pan, Y., Birdsey, R., Fang, J., Houghton, R., Kauppi, P., Kurz, W., Phillips, O., Shvidenko, A., Lewis, S., Canadell, J., Ciais, P., Jackson, R., Pacala, S., McGuire, A., Piao, S., Rautiainen, A., Sitch, S., and Hayes, D.: A large and persistent carbon sink in the world's forests. Science, 333(6045), 988–993, doi: 10.1126/science.1201609, 2011.

Pan, Y., Birdsey, R., Phillips, O., and Jackson, R.: The structure, distribution, and biomass of the world's forests. Annu. Rev. Ecol. Syst., 44(1), 593–622, doi: 10.1146/annurev-ecolsys-110512-135914, 2013.

Panikov, N., Flanagan, P., Oechel, W., Mastepanov, M., and Christensen, T.: Microbial activity in soils frozen to below −39°C. Soil Biol. Biochem., 38, 785–794, doi: 10.1016/j.soilbio.2005.07.004, 2006.

Pappas, C., Maillet, J., Rakowski, S., Baltzer, J., Barr, A., Black, A., Fatichi, S., Laroque, C., Matheny, A., Roy, A., Sonnentag, O., and Zha, T.: Aboveground tree growth is a minor and decoupled fraction of boreal forest carbon input. Agr. Forest Meteorol., 290, 108030, doi: 10.1016/j.agrformet.2020.108030, 2020.

Parinussa, R., Holmes, T., and de Jeu, R.: Soil moisture retrievals from the WindSat spaceborne polarimetric microwave radiometer. IEEE T. Geosci. Remote, 50(7), 2683–2694, doi: 10.1109/TGRS.2011.2174643, 2012.

Parazoo, N., Arneth, A., Pugh, T., Smith, B., Steiner, N., Luus, K., Commane, R., Benmergui, J., Stofferahn, E., Liu, J., Rödenbeck, C., Kawa, R., Euskirchen, E., Zona, D., Arndt, K., Oechel, W., Miller, C.: Spring photosynthetic onset and net CO_2 uptake in Alaska triggered by landscape thawing. Global Change Biol., 24(8), 3416–3435, doi: 10.1111/gcb.14283, 2018.

Pastorello, G., Trotta, C., Canfora, E., et al.: The FLUXNET2015 dataset and the ONEFlux processing pipeline for eddy covariance data. Sci. Data, 7, 225, doi: 10.1038/s41597-020-0534-3, 2020.

Peng, C., Ma, Z., Lei, X., Zhu, Q., Chen, H., Wang, W., Liu, S., Li, W., Fang, X., and Zhou, X.: A drought-induced pervasive increase in tree mortality across Canada's boreal forests. Nat. Clim. Change, 1, 467–471, doi: 10.1038/nclimate1293, 2011.

Piao, S., Ciais, P., Friedlingstein, P., Peylin, P., Reichstein, M., Luyssaert, S., Margolis, H., Fang, J., Barr, A., Chen, A., Grelle, A., Hollinger, D., Laurila, T., Lindroth, A., Richardson, A., and Vesala, T.: Net carbon dioxide losses of northern ecosystems in response to autumn warming. Nature, 451(7174), 49-52, doi: 10.1038/nature06444, 2008.

Picard, G., Sandells, M., and Löwe, H.: SMRT : an active–passive microwave radiative transfer model for snow with multiple microstructure and scattering formulations (v1.0). Geosci. Model Dev., 11(7), 2763–2788, doi: 10.5194/gmd-11-2763-2018, 2018.

Pierce, L., Ulaby, F., Sarabandi, K., and Dobson, M.: Knowledge-based classification of polarimetric SAR images. IEEE T. Geosci. Remote, 31(5), 1081-1086, doi: 10.1109/36.312896, 1994.

Pierdicca, N., Davidson, M., Chini, M., Dierking, W., Djavidnia, S., Haarpaintner, J., Hajduch, G., Laurin, G., Lavalle, M., López-Martínez, C., Nagler, T., and Su, B.: The Copernicus L-band SAR mission ROSE-L (Radar Observing System for Europe. Proc. Spie, Microwave Remote sensing for Environmental Monitoring III, 111540E, 2019.

Pierrat, Z., Nehemy, M. F., Roy, A., Magney, T., Parazoo, N., Laroque, C., Pappas, C., Sonnentang, O., Grossman, K., Bowling, D.R., Seibt, U., Ramirez, A., Johnson, B., Helgason, W., Barr, A., and Stutz, J.: Tower-based Remote sensing reveals mechanisms behind a two-phased spring transition in a mixed species boreal forest. J. Geophys. Res.: Biogeosciences. 126: e2020JG006191, doi: 10.1029/2020JG006191, 2020.

Potapov, P., Hansen, M., Stehman, S., Loveland, T., and Pittman, K.: Combining MODIS and Landsat imagery to estimate and map boreal forest cover loss. Remote Sens. Environ., 112(9), 3708-3719, doi: 10.1016/j.rse.2008.05.006, 2008.

Prince, M., Roy, A., Brucker, L., Royer, A., Youngwood, K., and Zhao, T.: Northern hemisphere surface freeze/thaw product from Aquarius L-band radiometers. Earth Syst. Sci. Data, 10(4), 2055–2067, doi: 10.1117/12.2534743, 2018.

Prince, M., Roy, A., Royer, A., and Langlois, A.: Timing and spatial variability of fall soil freezing in boreal forest and its effect on SMAP L-band radiometer measurements. Remote Sens. Environ., 231, 111230, doi: 10.1016/j.rse.2019.111230, 2019.

Pulliainen, J., Grandell, J., and Hallikainen, M.: Retrieval of surface temperature in boreal forest zone from SSM/I data. IEEE T. Geosci. Remote, 35(5), 1188–1200, doi: 10.1109/36.628786, 1997.

Pulliainen, J.: Mapping of snow water equivalent and snow depth in boreal and sub-arctic zones by assimilating space-borne microwave radiometer data and ground-based observations. Remote Sens. Environ., 101, 257-269, doi: 10.1016/j.rse.2006.01.002, 2006.

Pulliainen, J., Aurela, M., Laurila, T., Aalto, T., Takala, M., Salminen, M., Kulmala, M., Barr, A., Heimann, M., Lindroth, A., Laaksonen, A., Derksen, C., Mäkelä, A., Markkanen, T., Lemmetyinen, J., Susiluoto, J., Dengel, S., Mammarella, I., Tuovinen, J.-P., and Vesala, T.: Early snowmelt significantly enhances boreal springtime carbon uptake. P. Natl. A. Sci. USA, 114(42), 11081–11086, doi: 10.1073/pnas.1707889114, 2017.

Pulliainen, J., Luojus, K., Derksen, C., Mudryk, L., Lemmetyinen, J., Salminen, M., Ikonen, J., Takala, M., Cohen, J., Smolander, T., and Norberg, J.: Patterns and trends of Northern Hemisphere snow mass from 1980 to 2018. Nature, 581, 294–298, doi: 10.1038/s41586-020-2258-0, 2020.

Quegan, S., Le Toan, T., Chave, J., Dall, J., Exbrayat, J.-F., Minh, D., Lomas, M., Mariotti D'Alessandro, M. , Paillou, P., Papathanassiou, K., Rocca, F., Saatchi, S., Scipal, K., Shugart, H., Smallman, L., Soja, M., Tebaldini, S., Ulander, L., Vllard, L., and Williams, M.: The European Space Agency BIOMASS mission: Measuring forest above-ground biomass from space. Remote Sens. Environ., 227, 44–60, doi: 10.1016/j.rse.2019.03.032, 2019.

Rafat, A., Rezanezhad, F., Quinton, W.L., Humphreys, E.R., Webster, K., and Van Cappellen, P.: Non-growing season carbon emissions in a northern peatland are projected to increase under global warming. Commun. Earth Environ. 2, 111.

Ranson, K., and Sun, G.: Effects of environmental conditions on boreal forest classification and biomass estimates with SAR. IEEE T. Geosci. Remote, 38(3), 1242–1252, doi: 10.1109/36.843016, 2020.

Rantanen, M., Karpechko, A. Y., Lipponen, A., Nordling, K., Hyvärinen, O., Ruosteenoja, K., Vihma, T. and Laaksonen, A.: The Arctic has warmed nearly four times faster than the globe since 1979. Commun. Earth Environ., 3, 168, doi: 10.1038/s43247-022-00498-3, 2022.

Rautiainen, K., Lemmetyinen, J., Pulliainen, J., Vehviläinen, J., Drusch, M., Kontu, A., Kainulainen, J., and Seppanen, J.: L-band radiometer observations of soil processes at boreal and sub- Arctic environments. IEEE T. Geosci. Remote, 50(5), 1483–1497, doi: 10.1109/TGRS.2011.2167755, 2012.

Rautiainen, K., Parkkinen, T., Lemmetyinen, J., Schwank, M., Wiesmann, A., Ikonen, J., Derksen, C., Davydov, S., Davydova, A., Boike, J., and Langer, M.: SMOS prototype algorithm for detecting autumn soil freezing. Remote Sens. Environ., 180, 346–360, doi: 10.1016/j.rse.2016.01.012, 2016.

Rautiainen, K., Comite, D., Cohen, J., Cardellach, E., Unwin, M., and Pierdicca, N.: Freeze–Thaw Detection Over High-Latitude Regions by Means of GNSS-R Data. IEEE Trans. Geosci. Remote Sens., 60, 1-13, 4302713, doi: 10.1109/TGRS.2021.3125315, 2022.

Ravn, N., Elberling, B., and Michelsen, A.: Arctic soil carbon turnover controlled by experimental snow addition, summer warming and shrub removal. Soil Biol. Biochem., 142, 107698, doi: 10.1016/j.soilbio.2019.107698, 2020.

Rodríguez-Fernández, N. J., Mialon, A., Mermoz, S., Bouvet, A., Richaume, P., Al Bitar, A., Al-Yaari, A., Brandt, M., Kaminski, T., Le Toan, T., Kerr, Y., and Wigneron, J.-P.: An evaluation of SMOS L-band vegetation visible depth (L-VOD) data sets: high sensitivity of L-VOD to above-ground biomass in Africa. Biogeosciences, 15(14), 4627–4645, doi: 10.5194/bg-15-4627-2018, 2018.

Rodríguez-Fernández, N., Al Bitar, A., Colliander, A., and Zhao, T.: Soil moisture remote sensing across scales. Remote Sens., 11(2), 190, doi: 10.3390/rs11020190, 20190a.

Rodríguez-Fernández, N., Mialon, A., Merlin, O., Suere, C., Cabot, F., Khazaal, A., Costeraste, J., Palacin, B., Rodriguez-Suquet, R., Tournier, T., Decoopman, T., Colom, M., Morel, J.-M., and Kerr, Y.: SMOS-HR: A high resolution L-Band passive radiometer for earth science and applications. IGARSS 2019 - 2019 IEEE International Geoscience and Remote sensing Symposium, Yokohama, Japan, 28 July – 2 August 2019, 8392-8395, doi: 10.1109/IGARSS.2019.8897815, 2019b.

Rogers, M., Sullivan, P. and Welker, J.: Evidence of nonlinearity in the response of net ecosystem CO_2 exchange to increasing levels of winter snow depth in the high Arctic of Northwest Greenland. Arct. Antarct. Alp. Res., 43(1), 95-106, doi: 10.1657/1938-4246-43.1.95, 2010.

Rosen, P., Hensley, S., Shaffer, S., Veilleux, L., Chakraborty, M., Misra, T., Bhan, R., Sagi, R., and Satish, R.: The NASA-ISRO SAR mission - An international space partnership for science and societal benefit. 2015 IEEE Radar Conference (RadarCon), Arlington, United States, 10-15 May 2015, 1610-1613, doi: 10.1109/RADAR.2015.7131255, 2015.

Rosen, P., Hensley, S., Shaffer, S., Edelstein, W., Kim, Y., Kumar, R., Misra, T., Bhan, R., Satish, R., and Sagi, R.: An update on the NASA-ISRO dual-frequency DBF SAR (NISAR) mission. 2016 IEEE International Geoscience and Remote sensing Symposium (IGARSS), Beijing, China, 10-15 July 2016, 2106-2108, doi: 10.1109/IGARSS.2016.7729543, 2016.

Roy, A., Royer, A., Wigneron, J.-P., Langlois, A., Bergeron, J., and Cliche, P.: A simple parameterization for a boreal forest radiative transfer model at microwave frequencies. Remote Sens. Environ., 124, 371-383, doi: 10.1016/j.rse.2012.05.020, 2012.

Roy, A., Royer, A., and Hall, R.: Relationship between forest microwave transmissivity and structural parameters for the Canadian boreal forest. IEEE Geosci. Remote S., 11(10), 1802-1806, doi: 10.1109/LGRS.2014.2309941, 2014.

Roy, A., Royer, A., Derksen, C., Brucker, L., Langlois, A., Mialon, A., and Kerr, Y.: Evaluation of spaceborne L-Band radiometer measurements for terrestrial freeze/thaw retrievals in Canada. IEEE J. Sel. Top. Appl.8, 4442–4459, doi: 10.1109/JSTARS.2015.2476358, 2015.

Roy, A., Toose, P., Williamson, M., Rowlandson, T., Derksen, C., Royer, A., Berg, A., Lemmetyinen, J., and Arnold, L.: Response of L-Band brightness temperatures to freeze/thaw and snow dynamics in a prairie environment from ground-based radiometer measurements. Remote Sens. Environ., 191, 67-80, doi: 10.1016/j.rse.2017.01.017, 2017a.

Roy, A., Toose, P., Derksen, C., Rowlandson, T., Berg, A., Lemmetyinen, J., Royer, A., Tetlock, E., Helgason, W., and Sonnentag, O.: Spatial Variability of L-Band Brightness Temperature during Freeze/Thaw Events over a Prairie Environment. Remote Sens., 9, 894, doi: 10.3390/rs9090894, 2017b.

Roy, A., Toose, P., Mavrovic, A., Pappas, C., Royer, C., Derksen, C., Berg, A., Rowlandson, T., El-Amine, M., Barr, A., Black, A., Langlois, A., and Sonnentag, O.: L-Band response to freeze/thaw in a boreal forest stand from ground- and tower-based radiometer observations. Remote Sens. Environ., 237, 111542, doi: 10.1016/j.rse.2019.111542, 2020.

Royer, A., and Poirier, S.: Surface temperature spatial and temporal variations in North America from homogenized satellite SMMR-SSM/I microwave measurements and reanalysis for 1979–2008. J. Geophys. Res., 115, D08110, doi: 10.1029/2009JD012760, 2010.

Royer, A., Roy, A., Jutras, S., and Langlois, A.: Review article: Performance assessment of radiation-based field sensors for monitoring the water equivalent of snow cover (SWE). Cryosphere, 15, 5079–5098, doi: 10.5194/tc-15-5079-2021, 2021.

Saatchi, S., and Rignot, E.: Classification of boreal forest cover types using SAR images. Remote Sens. Environ., 60, 270–281, doi: 10.1016/S0034-4257(96)00181-2, 1997.

Saberi, N., Kelly, R., Flemming, M., and Li, Q.: Review of snow water equivalent retrieval methods using spaceborne passive microwave radiometry. Int. J. Remote Sens., 41(3), 996-1018, doi: 10.1080/01431161.2019.1654144, 2020.

Santoro, M., and Cartus, O.: Research pathways of forest above-ground biomass estimation based on SAR backscatter and interferometric SAR observations. Remote Sens., 10(4), 608, doi: 10.3390/rs10040608, 2018.

Santoro, M., Cartus, O., Mermoz, S., Bouvet, A., Le Toan, T., Carvalhais, N., Rozendaal, D., Herold, M., Avitabile, V., Shaun, Q., Carreiras, J., Rauste, Y., Balzter, H., Schmullius, C., and Seifert, F.: A detailed portrait of the forest aboveground biomass pool for the year 2010 obtained from multiple Remote sensing observations. Proceedings of the EGU General Assembly Conference Abstracts, Vienna, Austria, 8–13 April 2018, 20, 18932, 2018.

Schär, C., Fuhrer, O., Arteaga, A., Ban, N., Charpilloz, C., Di Girolamo, S., Hentgen, L., Hoefler, T., Lapillonne, X., Leutwyler, D., Osterried, K., Panosetti, D., Rüdisühli, S., Schlemmer, L., Schulthess, T., Sprenger, M., Ubbiali, S., and Wernli, H.: Kilometer-scale climate models: prospects and challenges. B. Am. Meteorol. Soc., 101(5), E567-E587, doi: 10.1175/BAMS-D-18-0167.1, 2020.

Schädel, C., Bader, M., Schuur, E., Biasi, C., Bracho, R., Čapek, P., De Baets, S., Diáková, K., Ernakovich, J., Estop-Aragones, C., Graham, D., Hartley, I., Iversen, C., Kane, E., Knoblauch, C., Lupascu, M., Martikainen, P., Natali, S., Norby, R., O'Donnell, J., Chowdhury, T., Šantrůčková, H., Shaver, G., Sloan, V., Treat, C., Turetsky, M., Waldrop, M., and Wickland, K.: Potential carbon emissions dominated by carbon dioxide from thawed permafrost soils. Nat. Clim. Change, 6, 950–953, doi: 10.1038/nclimate3054, 2016.

Schaefer, K., Schmidt, N., Schuur, E., Semenchuk, P., Shaver, G., Sonnentag, O., Starr, G., Treat, C., Waldrop, M., Wang, Y., Welker, J., Wille, C., Xu, Zhang, Z., Zhuang, Q., and Zona, D.: Large loss of CO_2 in winter observed across the northern permafrost region. Nat. Clim. Change, 9, 852–857, doi: 10.1038/s41558-019-0592-8, 2019.

Schlund, M., Scipal, K., and Quegan, S.: Assessment of a power law relationship between P-band SAR backscatter and aboveground biomass and its implications for BIOMASS mission performance. IEEE J. Sel. Top. Appl., 11(10), 3538-3547, doi: 10.1109/JSTARS.2018.2866868, 2018.

Schuur, E., McGuire, A., Schädel, C., Grosse, G., Harden, J., Hayes, D., Hugelius, G., Koven, C., Kuhry, P., Lawrence, D., Natali, S., Olefeldt, D., Romanovsky, V., Schaefer, K., Turetsky, M., Treat, C., and Vonk, J.: Climate change and the permafrost carbon feedback. Nature, 520, 171-179, doi: 10.1038/nature14338, 2015.

Seiler, C., Melton, J., Arora, V., Sitch, S., Friedlingstein, P., Anthoni, P., Goll, D., Jain, A., Joetzjer, E., Lienert, S., Lombardozzi, D., Luyssaert, S., Nabel, J., Tian, H., Vuichard, N., Walker, A., Yuan, W. and Zaehle, S.: Are terrestrial biosphere models fit for simulating the global land carbon sink? JAMES, 14(5), e2021MS002946, doi: 10.1029/2021MS002946, 2022.

Shi, J., Xiong, C., and Jiang, L.: Review of snow water equivalent microwave remote Sensing. Science China Earth Sciences, 59(4), 731–745, doi: 10.1007/s11430-015-5225-0, 2016.

1570

Sitch, S., McGuire, D., Kimball, J., Gedney, N., Gamon, J., Engstrom, R., Wolf, A., Zhuang, Q., Clein, J., and McDonald, K.: Assessing the carbon balance of circumpolar Arctic tundra using Remote sensing and process modelling. Ecol. Appl., 17(1), 213-234, doi: 10.1890/1051-0761(2007)017[0213:ATCBOC]2.0.CO;2, 2007.

1575 Sniderhan, A., Mamet, S., and Baltzer, J.: Non-uniform growth dynamics of a dominant boreal tree species (*Picea mariana*) in the face of rapid climate change. Can. J. Forest Res., 51(4), 565-572, doi: 10.1139/cjfr-2020-0188, 2021.

Stefan, V.-G., Indrio, G., Escorihuela, M.-J., Quintana-Sehuì, P., and Villar, J., M.: High-resolution SMAP-derived root-
1580   zone soil moisture using an exponential filter model calibrated per land cover type. Remote Sens., 13, 1112, 2021.

Sturm, M., Holmgren, J., König, M., and Morris, K.: The thermal conductivity of seasonal snow. J. Glaciol., 43(143), 26–41, doi: 10.3189/s0022143000002781, 1997.

1585

Sturm, M., Schimel, J., Michaelson, G., Welker, J., Oberbauer, S., Liston, G., Fahnestock, J., and Romanovsky, V.: Winter biological processes could help convert arctic tundra to shrubland, Bioscience, 55, 17–26, doi: 10.1641/0006-3568(2005)055[0017:WBPCHC]2.0.CO;2, 2005.

1590 Sulla-Menashe, D., Woodcock, C., and Friedl, M.: Canadian boreal forest greening and browning trends: an analysis of biogeographic patterns and the relative roles of disturbance versus climate drivers. Environ. Res. Lett., 13(1), 014007, doi: 10.1088/1748-9326/aa9b88, 2018.

Suni, T., Berninger, F., Markkanen, T., Keronen, P., Rannik, Ü., and Vesala, T.: Interannual variability and timing of
1595   growing-season CO_2 exchange in a boreal forest. J. Geophys. Res.: Atmospheres, 108(D9), 4265, doi: 10.1029/2002JD002381, 2003.

Savtchenko, A., Ouzounov, D., Ahmad, S., Acker, J., Leptoukh, G., Koziana, J., and Nickless, D.: Terra and Aqua MODIS products available from NASA GES DAAC. Adv. Space Res., 34(4), 710-714, doi:
1600   10.1016/j.asr.2004.03.012, 2004.

Takala, M., Luojus, K., Pulliainen, J., Derksen, C., Lemmetyinen, J., Kärnä, J.-P., Koskinen, J., and Bojkov, B.: Estimating northern hemisphere snow water equivalent for climate research through assimilation of space-borne radiometer data and ground-based measurements. Remote Sens. Environ., 115(12), 3517–3529, doi:
1605   10.1016/j.rse.2011.08.014, 2011.

Tanja, S., Berninger, F., Vesala, T., Markkanen, T., Hari, P., Mäkelä, A., Ilvesniemi, H., Hänninen, H., Nikinmaa, E., Huttula, T., Laurila, T., Aurela, M., Grelle, A., Lindroth, A., Arneth, A., Shibistova, O., and Lloyd, J.: Air temperature triggers the commencement of evergreen boreal forest photosynthesis in spring. Global Change
1610   Biol., 9, 1410-1426, 2003, doi: 10.1046/j.1365-2486.2003.00597.x, 2003.

Tarnocai, C., Canadell, J., Schuur, E., Kuhry, P., Mazhitova, G., and Zimov, S.: Soil organic carbon pools in the northern circumpolar permafrost region. Gobal Biogeochem. Cy., 23(2), GB2023, doi: 10.1029/2008GB003327, 2009.

1615 Tebaldini, S., Ho Tong Minh, D., Mariotti d'Alessandro, M., Villard, L., Le Toan, T., and Chave, J.: The status of technologies to measure forest biomass and structural properties: state of the art in SAR tomography of tropical forests. Surv. Geophys., 40, 779-801, doi: 10.1007/s10712-019-09539-7, 2019.

Tedesco, M., and Jeyaratnam, J.: A new operational snow retrieval algorithm applied to historical AMSR-E brightness
1620 temperatures. Remote Sens., 8(12), 103, doi: 10.3390/rs8121037, 2016.

Tei, S., and Sugimoto, A.: Excessive positive response of model-simulated land net primary production to climate changes over circumboreal forests. Plant-Environment Interactions, 1(2), 102-121, doi: 10.1002/pei3.10025, 2020.

1625

Tenkanen, M., Tsuruta, A., Rautiainen, K., Kangasaho, V., Ellul, R., and Aalto, T.: Utilizing earth observations of soil freeze/thaw data and atmospheric concentrations to estimate cold season methane emissions in the Northern high latitudes. Remote Sens., 13(24), 5059, doi: 10.3390/rs13245059, 2021.

1630 Teubner, I., Forkel, M., Jung, M., Liu, Y., Miralles, D., Parinussa, R., van der Schalie, R., Vreugdenhil, M., Schwalm, C., Tramontana, G., Camps-Valls, G., and Drigo, W.: Assessing the relationship between microwave vegetation visible depth and gross primary production. Int. J. Appl. Earth Obs., 65, 79–91, doi: 10.1016/j.jag.2017.10.006, 2018.

1635 Teubner, I., Forkel, M., Camps-Valls, G., Jung, M., Miralles, D., Tramontana, G., van der Schalie, R., Vreugdenhil, Mösinger, L., and Dorigo, W.: A carbon sink-driven approach to estimate gross primary production from microwave satellite observations. Remote Sens. Environ., 229, 100–113, doi: 10.1016/j.rse.2019.04.022, 2019.

Tian, F., Brandt, M., Liu, Y., Verger, A., Tagesson, T., Diouf, A., Rasmussen, K., Mbow, C., Wang, Y., and Fensholt,
1640 R.: Remote sensing of vegetation dynamics in drylands: Evaluating vegetation visible depth (VOD) using AVHRR NDVI and in situ green biomass data over West African Sahel. Remote Sens. Environ., 177, 265–276, doi: 10.1016/j.rse.2016.02.056, 2016.

Tomiyasu, K.: Tutorial Review of Synthetic-Aperture Radar (SAR) with Applications to Imaging of Ocean Surface. P.
1645 IEEE, 66(5), 563-583, doi: 10.1109/PROC.1978.10961, 1978.

Topp, G., Davis, J., and Annan, A.: Electromagnetic determination of soil water content: Measurements in coaxial transmission lines. Water Resour. Res., 16(3), 574-582, doi: 10.1029/WR016i003p00574, 1980.

1650 Topp, E. and Pattey, E.: Soils as sources and sinks for atmospheric methane. Can. J. Soil Sci., 77(2), 167-177, doi: https://doi.org/10.4141/S96-107, 1997.

Touati, C., Ratsimbazafy, T., Ludwig, R., and Bernier, M.: New approaches for removing the effect of water damping on SMAP freeze/thaw mapping. Can. J. Remote Sens., 45(3-4), 405-422, doi: 10.1080/07038992.2019.1638236, 2019.

Töyrä, J., Pietroniro, A., and Martz, L.: Multisensor hydrologic assessment of a freshwater wetland. Remote Sens. Environ., 75, 162–173, doi: 10.1016/s0034-4257(00)00164-4, 2001.

Tu, Q., Hase, F., Blumenstock, T., Kivi, R., Heikkinen, P., Sha, M. K., Raffalski, U., Landgraf, J., Lorente, A., Borsdorff, T., Chen, H., Dietrich, F., and Chen, J.: Intercomparison of atmospheric CO2 and CH4 abundances on regional scales in boreal areas using Copernicus Atmosphere Monitoring Service (CAMS) analysis, COllaborative Carbon Column Observing Network (COCCON) spectrometers, and Sentinel-5 Precursor satellite observations. Atmos. Meas. Tech., 13, 4751-4771, doi: 10.5194/amt-13-4751-2020, 2020.

Tucker, C. J.: Red and photographic infrared linear combinations for monitoring vegetation. Remote Sens. Environ., 8(2), 127–150, doi: 10.1016/0034-4257(79)90013-0, 1979.

Turner, D., Ollinger, S., and Kimball, J.: Integrating remote sensing and ecosystem process models for landscape- to regional-scale analysis of the carbon cycle. Bioscience, 54(6), 573-584, doi: 10.1641/0006-3568(2004)054[0573:IRSAEP]2.0.CO;2, 2004.

Ulaby, F., Moore, R., and Fung, A.: Microwave Remote Sens.-Basel: Active and Passive, Vol. II – Radar remote sensing and surface scattering and emission theory. Addison-Wesley Publishing Company, Advanced Book Program/World Science Division, Norwood, Massachusetts, United-States, 1982.

Ulaby, F., Moore, R., and Fung, A.: Microwave Remote Sens.: Active and Passive. Vol. III. From theory to applications. Artech House Publishers, Norwood, Massachusetts, United-States, 1986.

Ulaby, F., Sarabandi, K., McDonald, K., Whitt, M., and Dobson, M. C.: Michigan microwave canopy scattering model. Int. J. Remote Sens., 11(7), 1223-1253, doi: 10.1080/01431169008955090, 1990.

Ullmann, T., Schmitt, A., Roth, A., Duffe, J., Dech, S., Hubberten, H.-W., and Baumhauer, R.: Land cover characterization and classification of arctic tundra environments by means of polarized synthetic aperture X- and C-Band radar (PolSAR) and Landsat 8 multispectral imagery—Richards Island, Canada. Remote Sens., 6, 8565–8593, doi: 10.3390/rs6098565, 2014.

Virkkala, A.-M., Aalto, J., Rogers, B., Tagesson, T., Treat, C., Natali, S., Watts, J., Potter, S., Lehtonen, A., Mauritz, M., Schuur, E., Kochendorfer, J., Zona, D., Oechel, W., Kobayashi, H., Humphreys, E., Goeckede, M., Iwata, H., Lafleur, P., Euskirchen, E., Bokhorst, S., Marushchak, M., Martikainen, P., Elberling, B., Voigt, C., Biasi, C., Sonnentag, O., Parmentier, F.-J., Ueyama, M., Celis, G., St.Louis, V., Emmerton, C., Peichl, M., Chi, J., Järveoja, J., Nilsson, M., Oberbauer, S., Torn, M., Park, S.-J., Dolman, H., Mammarella, I., Chae, N., Poyatos, R., López-Blanco, E., Christensen, T., Kwon, M., Sachs, T., Holl, D., and Luoto, M.: Statistical upscaling of

ecosystem CO_2 fluxes across the terrestrial tundra and boreal domain: Regional patterns and uncertainties. Global Change Biol., 27(17), 4040-4059, doi: 10.1111/gcb.15659, 2021.

Vittucci, C., Vaglio Laurin, G., Tramontana, G., Ferrazzoli, P., Guerriero, L., and Papale, D.: Vegetation visible depth at L-band and above ground biomass in the tropical range: Evaluating their relationships at continental and regional scales. Int. J. Appl. Earth Obs., 77, 151–161, doi: 10.1016/j.jag.2019.01.006, 2019.

Wagner, W., Hahn, S., Kidd, R., Melzer, T., Bartalis, Z., Hasenauer, S., Figa-Saldaña, J., de Rosnay, P., Jann, A., Schneider, S., Komma, J., Kubu, G., Brugger, K., Aubrecht, C., Züger, J., Gangkofner, U., Kienberger, S., Brocca, L., Wang, Y., Blöschl, G., Eitzinger, J., and Steinnocher, K.: The ASCAT soil moisture product: A review of its specifications, validation results, and emerging applications. Meteorol. Z., 22(1), 5-33, doi: 10.1127/0941-2948/2013/0399, 2013.

Walker, X., and Johnstone, J.: Widespread negative correlations between black spruce growth and temperature across topographic moisture gradients in the boreal forest. Environ. Res. Lett., 9(6), 064016, doi: 10.1088/1748-9326/9/6/064016, 2014.

Walker, X., Rogers, B., Baltzer, J., Cumming, S., Day, N., Goetz, S., Johnstone, J., Schuut, E., Turetsky, M., and Mack, M.: Cross-scale controls on carbon emissions from boreal forest megafires. Global Change Biol., 24(9), 4251-4265, doi: 10.1111/gcb.14287, 2018.

Walker, X., Baltzer, J., Cumming, S., Day, N., Ebert, C., Goetz, S., Johnstone, J., Potter, S., Rogers, B., Schuut, E., Turetsky, M., and Mack, M.: Increasing wildfires threaten historic carbon sink of boreal forest soils. Nature, 572, 520-523, doi: 10.1038/s41586-019-1474-y, 2019.

Walker, X., Rogers, B., Veraverbeke, S., Johnstone, J., Baltzer, J., Barrett, K., Bourgeau-Chavez, L., Day, N., de Groot, W., Dieleman, C., Goetz, S., Hoy, E., Jenkins, L., Kane, E., Parisien, M.-A., Potter, S., Schuur, E., Turetsky, M., Whitman, E., and Mack, M.: Fuel availability not fire weather controls boreal wildfire severity and carbon emissions. Nat. Clim. Change, 10, 1130-1136, doi: 10.1038/s41558-020-00920-8, 2020.

Wang, J., Sulla-Menashe, D., Woodcock, C., Sonnentag, O., Keeling, R., and Friedl, M.: Extensive land cover change across Arctic-Boreal Northwestern North America from disturbance and climate forcing. Global Change Biol., 26(3), 807-822, doi: 10.1111/gcb.14804, 2019.

Washington, W., Buja, L., and Craig, A.: The computational future for climate and Earth system models: on the path to petaflop and beyond. Philos. T. Roy. Soc. A., 367(1890), 833-846, doi: 10.1098/rsta.2008.0219, 2009.

Watts, J., Kimball, J., Bartsch, A., and McDonald, K.: Surface water inundation in the boreal-Arctic: potential impacts on regional methane emissions. Environ. Res. Lett., 9, 075001, doi: 10.1088/1748-9326/9/7/075001, 2014.

Webb, E., Schuur, E., Natali, S., Oken, K., Bracho, R., Krapek, J., Risk, D., and Nickerson, N.: Increased wintertime
1735   CO_2 loss as a result of sustained tundra warming. J. Geophys. Res.-Biogeo., 121(2), 249-265, doi:
   10.1002/2014JG002795, 2016.

Welker, J., Fahnestock, J., and Jones, M.: Annual CO_2 flux in dry and moist Arctic tundra: field responses to increases
   in summer temperatures and winter snow depth. Climatic Change, 44, 139–150, doi:
1740   10.1023/A:1005555012742, 2000.

Whitcomb, J., Moghaddam, M., McDonald, K., Kellndorfer, J., and Podest, E.: Mapping vegetated wetlands of Alaska
   using L-band radar satellite imagery. Can. J. Remote Sens., 35(1), 54–72, doi: 10.5589/m08-080, 2009.

1745 Wigneron, J.-P., Kerr, Y., Waldteufel, P., Saleh, K., Escorihuela, M.-J., Richaume, P., Ferrazzoli, P., de Rosnay, P.,
   Gurneye, R., Calvet, J.-C., Grant, J., Guglielmetti, M., Hornbuckle, B., Mätzler, C., Pellarin, T., and Schwank,
   M.: L-band Microwave Emission of the Biosphere (L-MEB) Model: Description and calibration against
   experimental data sets over crop fields. Remote Sens. Environ., 107(4), 639-655, doi:
   10.1016/j.rse.2006.10.014, 2007.
1750

Wigneron, J.-P., Li, X., Frappart, F., Fan, L., Al-Yaari, A., De Lannoy, G., Liu, X., Wang, M., Le Masson, E., and Moisy,
   C.: Overview of the SMOS-IC data recordofsoil moisture and L-VOD: Historic development, applications and
   perspectives. Remote Sens. Environ., 254, 112238, doi: 10.1016/j.rse.2020.112238, 2021.

1755 Wohlfahrt, G., Gerdel, K., Migliavacca, M., Rotenberg, E., Tatarinov, F., Müller, J., Hammerle, A., Julitta, T., Spielmann,
   F., and Yakir, D.: Sun-induced fluorescence and gross primary productivity during a heat wave. Sci. Rep.-UK.,
   8, 14169, doi: 10.1038/s41598-018-32602-z, 2018.

Wu, M., Scholze, M., Kaminski, T., Voßbeck, M., and Tagesson, T.: Using SMOS soil moisture data combining CO2
1760   flask samples to constrain carbon fluxes during 2010–2015 within a Carbon Cycle Data Assimilation System
   (CCDAS). Remote Sens. Environ., 240, 111719, doi: 10.1016/j.rse.2020.111719, 2020.

Wulder, M., Roy, D., Radeloff, V., Loveland, T., Anderson, M., Johnson, D., Healey, S., Zhu, Z., Scambos, T., Pahlevan,
   N., Hansen, M., Gorelick, N., Crawford, C., Masek, J., Hermosilla, White, J., Belward, A., Schaaf, C.,
1765   Woodcock, C., Huntington, J., Lymburner, L., Hostert, P., Gao, F., Lyapustin, A., Pekel, J.-F., Strobl, P. and
   Cook, B.: Fifty years of Landsat science and impacts. Remote Sens. Environ., 280, 113195, doi:
   0.1016/j.rse.2022.113195, 2022.

Xian, D., Zhang, P., Gao, L., Sun, R., Zhang, H., and Jia, X.: Fengyun Meteorological Satellite Products for
1770   Earth System Science Applications. Adv. Atmos. Sci., 38, 1267–1284, doi:10.1007/s00376-021-
   0425-3, 2021.

Xiao, J., Chevallier, F., Gomez, C., Guanter, L., Hicke, J., Huete, A., Ichii, K., Nih, W., Pang, Y., Rahman, A., Sun, G., Yuan, W., Zhang, L., and Zhang, X.: Remote sensing of the terrestrial carbon cycle: A review of advances over 50 years. Remote Sens. Environ., 233, 111383, doi: 10.1016/j.rse.2019.111383, 2019.

Xu, X., Derksen, C., Yueh, S. Dunbar, R., and Colliander, A.: Freeze/thaw detection and validation using Aquarius' L-Band backscattering data. IEEE J. Sel. Top. Appl., 9, (4),1370-1381, doi: 10.1109/JSTARS.2016.2519347, 2016.

Yang, W., Meng, H., Ferraro, R., Moradi, I., and Devaraj, C.: Cross-Scan asymmetry of AMSU-A window channels: characterization, correction, and verification. IEEE T. Geosci. Remote, 51(3), 1514–1530, doi: 10.1109/TGRS.2012.2211884, 2013.

Yi, Y., Kimball, J., Jones, L., Reichle, R., Nemani, R., and Margolis, H.: Recent climate and fire disturbance impacts on boreal and arctic ecosystem productivity estimated using a satellite-based terrestrial carbon flux model. J. Geophys. Res.-Biogeo., 118, 606–622, doi: 10.1002/jgrg.20053, 2013.

Yi, Y., Chen, R., Kimball, J., Moghaddam, M., Xu, X., Euskirchen, E., Das, N., and Miller, C.: Potential satellite monitoring of surface organic soil properties in arctic tundra from SMAP. Water Resour. Res., 58(4), e2021WR030957, doi: 10.1029/2021WR030957, 2022.

Yu, K., Han, S., Bu, J., An, Y., Zhou, Z., Wang, C., Tabibi, S., and Cheong, J. W.: Spaceborne GNSS Reflectometry. Remote Sens., 14, 1605, doi: 10.3390/rs14071605, 2022.

Zhang, L., Zhao, T., Jiang, L., and Zhao, S.: Estimate of phase transition water content in freeze–thaw process using microwave radiometer. IEEE T. Geosci. Remote, 48(12), 4248–4255, doi: 10.1109/TGRS.2010.2051158, 2010.

Zhang, Y. Song, C., Sun, G., Band, L., Noormets, A. and Zhang, Q.: Understanding moisture stress on light use efficiency across terrestrial ecosystems based on global flux and remote-sensing data. Biogeosciences, 120(10), 2053-2066, doi: 10.1002/2015JG003023, 2015.

Zhang, Q., and Cheng, J.: An empirical algorithm for retrieving land surface temperature from AMSR-E data considering the comprehensive effects of environmental variables. Earth and Space Science, 7(4), e2019EA001006, doi: 10.1029/2019EA001006, 2020.

Zhou, Z., Li, Z., Waldron, S., and Tanaka, A.: InSAR time series analysis of L-Band data for understanding tropical peatland degradation and restoration. Remote Sens., 11(21), 2592, doi: 10.3390/rs11212592, 2019.

Zona, D., Gioli, B., Commane, R. and Oechel, W.C.: Cold season emissions dominate the Arctic tundra methane budget. PNAS, 113(1), 40-45, doi: 10.1073/pnas.1516017113, 2015.

Zwieback, S., Bartsch, A., Melzer, T. and Wagner, W.: Probabilistic Fusion of Ku- and C-band Scatterometer Data for
1815   Determining the Freeze/Thaw State. IEEE T. Geosci. Remote, 50(7), 2583-2594, doi:
               10.1109/JSTARS.2015.2476358, 2011.

van Zyl, J.: Unsupervised classification of scattering behavior using radar polarimetry data. IEEE T. Geosci. Remote,
               27(1), 36-45, doi: 10.1109/36.20273, 1989.

1820

1825

1830

1835

1840

1845

1850

1855

12 Appendix A

Table A1: Microwave radiometers in the 1-100 GHz frequency range on sun-synchronous nearly polar orbits. Instrument specifications from Das and Paul (2015) and specific references.

Mission	SMMR	SSM/I SSMIS	AMSU-A	MSMR	AMSR AMSR-E	Windsat	MWRI	SMOS	Aquarius	AMSR-2	SMAP
Temporal coverage	1978 (Oct.) - 1987 (Aug.)	1987 (July) - Ongoing	1998 (Aug.) - Ongoing	1999 (May) – 2001 (Oct.)	2002 (June) – 2011 (Oct.)	2003 (Feb.) - Ongoing	2008 (May)- Ongoing	2010 (Jan.) - Ongoing	2011 (Aug.) - 2015 (June)	2012 (July) - Ongoing	2015 (April) - Ongoing
Frequency (GHz)	6.6, 10.7,18.0, 21.0 and 87.0	19.3, 22.2, 37.0 and 85.5	23.8, 31.4 and 89.0	6.6, 10.65, 18.0 and 21.0	6.925, 10.65, 18.7, 23.8, 36.5 and 89.0	6.8, 10.7, 18.7, 23.8 and 37.0	10.65, 18.7, 23.8,36.5 and 89.0	1.4	1.413 (3 of them)	6.925, 10.65, 18.7, 23.8, 36.5 and 89.0	1.41
IFOV (km)	148 × 95 91 × 59 55 × 41 46 × 30 27 × 18	69 × 43 60 × 40 37 × 28 15 × 13	48x48	150 × 144 75 × 72 50 × 36 50 × 36	75 × 43 51 × 29 27 × 16 32 × 18 14 × 8 6 × 4	60x40 38x25 27x16 20x12 13x8	51x85 30x50 27x45 18x30 9x15	43x43	94x76 120x84 156x97	62 × 35 42 × 24 22 × 14 19 × 11 12 × 7 5 × 3	36x47
Revisit coverage (days)	2	1	1-29	2	2	8	1	3	7	2	3
Swath widh (km)	822	1400	2200	1360	1445	950	1400	1000	390	1450	1000
Platform	Nimbus-7	Defense Meteorological Satellite Program	NOAA-15 to 19, Aqua, MetOp-A, B and C	Oceansat-1	ADEOS-II (AMSR) and Aqua (AMSR-E)	Coriolis	FengYun-3 constellation	SMOS	SAC-D	GCOM-W1	SMAP
Reference	Gloersen and Barath, 1977	Hollinger et al., 1990	Yang et al., 2012	Misra et al., 2002	Kawanishi et al., 2003	Gaiser et al., 2004	Xian et al., 2021	Kerr et al., 2010	Brucker et al., 2014	Maeda et al., 2016	Entekhabi et al., 2010

1860

Table A2: Microwave radar missions.

Mission	Launch date		Frequency (GHz)	Band	Spatial resolution (m)	Repeat cycle (days)
JERS-1	1992 (Feb.)	1998 (Oct.)	1.275	L	18	44
PALSAR / ALOS	2006 (Janv.)	2011 (May)	1.270	L	10-100	46
PALSAR / ALOS-2	2014 (May)	Ongoing	1.270	L	10-100	46
SOACOM-1a	2018 (Oct.)	Ongoing	1.275	L	7-100	16
SOACOM-1b	2020 (Oct.)	Ongoing	1.275	L	7-100	16
ERS-1	1991 (July)	2000 (March)	5.3	C	25-100	35
ERS-2	1995 (April)	2011 (July)	5.3	C	25-100	35
Sentinel-1a	2014 (April)	Ongoing	5.405	C	5-40	12
Sentinel-1b	2016 (April)	Ongoing	5.405	C	5-40	12
Radarsat-1	1995 (Nov.)	2013 (March)	5.3	C	8-100	24
Radarsat-2	2007 (Dec.)	Ongoing	5.405	C	3-100	24
Radarsat Constellation	2019 (June)	Ongoing	5.405	C	3-100	12
ASAR / ENVISAT	2002 (March)	2012 (May)	5.331	C	30-1000	35
ASCAT Constellation METOP-A METOP-B METOP-C	2006 (Oct.) 2012 (Sept.) 2018 (Nov.)	Ongoing	5.255	C	12.5-25 km	29
Cosmos-SkyMed Constellation	2007 (June) 2007 (Dec.) 2008 (Oct.) 2010 (Nov.)	Ongoing	9.6	X	1-100	16
TerraSAR-X	2007 (June)	Ongoing	9.65	X	0.5-40	11
TanDEM-X	2010 (June)	Ongoing	9.65	X	0.5-40	11
KOMPSAT-5	2018 (Aug.)	Ongoing	9.66	X	1-20	28
PAZ	2018 (Feb.)	Ongoing	9.65	X	1-15	11
ICEYE Constellation	2018 (Dec.; 2) 2019 (May; 1) 2019 (July; 2) 2020 (Sept.; 2) 2021 (Jan.; 3) 2021 (July; 4)	Ongoing	9.65	X	3	22
NSCAT / ADEOS	1996 (Aug.)	1997 (June)	13.995	K_u	25-50 km	41
QuickSCAT	1999 (June)	2009 (Nov.)	13.46	K_u	12.5-25 km	4